Unraveling dynamical controls on the North Pacific carbon sink

Jennifer M. Ayers[1,2] and M. Susan Lozier[1]

Received 9 June 2011; revised 14 November 2011; accepted 15 November 2011; published 26 January 2012.

[1] A broad swath across the North Pacific basin uptakes a disproportionately large amount of atmospheric CO_2 every year, with the region of most intense uptake located in the North Pacific transition zone, from ~30°N to 40°N–45°N. Though a net carbon sink on a mean annual basis, the region varies seasonally between a strong sink in winter and a neutral to weak source in summer. Herein we use observational carbon data to investigate processes regulating air-sea CO_2 flux in this region on seasonal and annual timescales by quantifying the impacts of temperature, biology, and physics on seawater pCO_2. Temperature effects dominate the pCO_2 signal seasonally, yet support only a portion of the annual CO_2 uptake in the region, via their impact on the solubility of CO_2 in seawater. Instead, processes removing carbon from surface waters dominantly support the region's uptake of CO_2 on annual timescales: the vertical export of organic carbon to depth, and the geostrophic advection of dissolved inorganic carbon laterally out of the region. We find the location of this carbon sink region, traditionally attributed to a combination of biological and temperature effects, to instead be driven by the steady geostrophic divergence of DIC at these latitudes.

Citation: Ayers, J. M., and M. S. Lozier (2012), Unraveling dynamical controls on the North Pacific carbon sink, *J. Geophys. Res.*, *117*, C01017, doi:10.1029/2011JC007368.

1. Background and Motivation

[2] The anthropogenic burning of fossil fuels, deforestation, modern agricultural practices, and other human activities have increased atmospheric carbon dioxide (CO_2) over the last century, raising it from 315 ppm in 1958 to its present value of 390 ppm in 2011 [*Keeling et al.*, 2001], driving an increase in global temperatures [*Brohan et al.*, 2006]. To date, the oceans have absorbed about 30% of these anthropogenic CO_2 emissions, thus decreasing the amount of CO_2 remaining in the atmosphere and in part mitigating global warming [*Sabine et al.*, 2004]. Though the oceans function as a net sink for atmospheric CO_2, the direction and magnitude of CO_2 exchange between the oceans and atmosphere varies considerably in space and time. Understanding processes regulating the oceanic uptake of CO_2 is critical to understanding both the resulting acidification of the oceans [*Byrne et al.*, 2010] and the future of Earth's climate.

[3] The oceanic regions between about 20–50° north and south in all basins act as net annual sinks for atmospheric carbon dioxide. The North Pacific basin in particular supports strong CO_2 uptake on a mean annual basis (Figure 1). Though the spatial extent of the sink is large, the strongest uptake occurs between ~30°N to 40–45°N basin wide [*Takahashi et al.*, 2002, 2009]. This region corresponds approximately to the North Pacific transition zone, sometimes defined as the region between the subtropical frontal zone and the subarctic frontal zone [*Roden*, 1991], but located dynamically in the northern reaches of the subtropical gyre [*Ayers and Lozier*, 2010]. Seasonally, this transition zone region varies between a strong sink in winter and a weak source in summer [*Ogawa et al.*, 2006; *Takahashi et al.*, 2009]. The region is of consequence not only as a strong annual carbon sink, but on decadal timescales as well: the western transition zone waters are maintaining a low sea surface pCO_2 (mean rate of increase 8.1 ± 3.0 μatm decade^{-1}), and therefore the potential to uptake atmospheric CO_2, more effectively than the rest of the North Pacific (mean open ocean rate of increase 12.0 ± 4.8 μatm decade^{-1}) [*Takahashi et al.*, 2006]. An understanding of regulatory controls on air-sea flux in the North Pacific is not only necessary to explain how the region sustains significant carbon uptake year after year, but may have broader relevance to other strong sink areas found in the same latitude belt in both hemispheres [*Takahashi et al.*, 1993, 2002, 2009].

[4] While it is widely recognized that temperature, biological production, and physical circulation all exert control on pCO_2 and thus air-sea carbon flux, the role of ocean circulation remains often unaddressed. *Takahashi et al.* [2002] separated observed changes in seawater pCO_2 into those due to temperature effects and those due to nontemperature effects on a global scale, revealing these effects to be of equal consequence in seasonal dynamics. Though the nontemperature effects on pCO_2 were referred to broadly as biological drawdown by the authors, the effects of physical ocean circulation also fell into this category, conflating the two. *Takahashi et al.* [1993, 2002, 2009] attributed the low sea surface pCO_2 in the strong carbon sink regions found

[1]Department of Earth and Ocean Sciences, Nicholas School of the Environment, Duke University, Durham, North Carolina, USA.
[2]Now at Institute for Marine and Antarctic Studies, University of Tasmania, Hobart, Tasmania, Australia.

0148-0227/12/2011JC007368

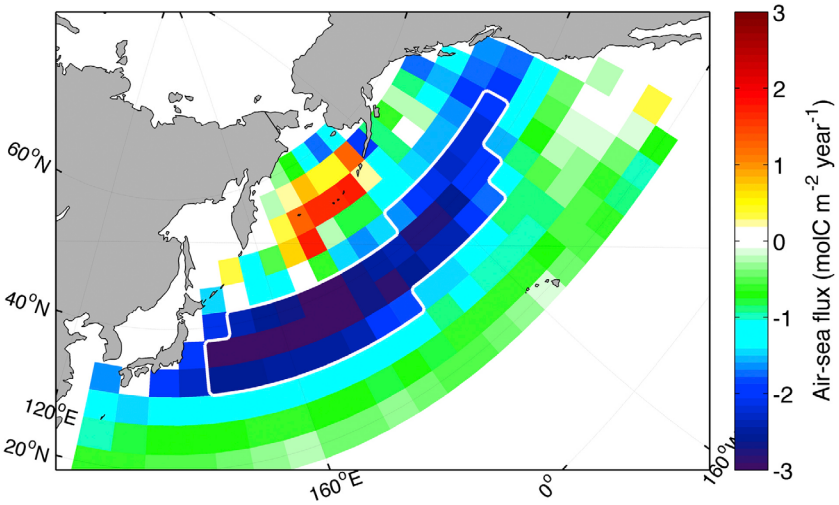

Figure 1. Mean annual air-sea carbon flux, from the *Takahashi et al.* [2010] data set. Negative values indicate oceanic uptake of CO_2; positive values indicate outgassing. White contour outlines the most intense portion of the sink region, identified roughly as transition zone waters where oceanic carbon uptake is greater than 1.7 mol C m^{-2} yr^{-1}. This contour defines the study domain, used for calculating regional averages reported throughout this work.

between ~20–50° latitude, including the North Pacific carbon sink region, to these temperature effects and biological drawdown: "In these areas, low pCO_2 waters are formed by the juxtaposition of the cooling of warm waters with the biological drawdown of pCO_2 in the nutrient-rich subpolar waters" [*Takahashi et al.*, 2002, p. 1608]. Strong westerly winds then increase the rate of air-sea carbon exchange over these waters, resulting in oceanic uptake of atmospheric carbon. Though temperature and biological processes clearly contribute to the nature of carbon dynamics in these latitudes, it is unclear how they alone would explain the location, seasonal variability, and annual persistence of these important carbon sinks. Thus this work aims to separate the non-temperature effects identified by *Takahashi et al.* [2002] into distinct biological and physical components, clarifying the role of ocean circulation in regulating sea surface pCO_2.

[5] Contradictory conclusions drawn in previous studies additionally lend importance to understanding the role of ocean circulation in carbon dynamics in the North Pacific carbon sink region. Based on their view of a temperature and biologically determined sink, *Takahashi et al.* [1993] conclude that an expansion of the subtropical gyre accompanied by a northerly shift in the gyre-gyre boundary would increase the strength of the sink. In contrast, *Rodgers et al.* [2008], based on their modeling study that includes ocean circulation explicitly, predict the reverse: a shrinking subtropical gyre and a southerly shift in the gyre-gyre boundary would increase the strength of the sink. This discrepancy in predictions highlights the need for a targeted study of processes controlling air-sea flux the North Pacific, explicitly considering the impact of physics as well as temperature and biology.

[6] In this study we use observational data to investigate processes regulating the ocean–atmosphere exchange of CO_2 in the North Pacific. We quantitatively estimate the impacts of temperature, biology, and physics on sea surface pCO_2 in the North Pacific carbon sink region on a monthly climatological basis. This allows us to identify processes controlling both the seasonal variability and the mean annual state of the sink. Finally, we return to the fundamental questions of interest: why the sink is located where it is, and what processes maintain it as such from one year to the next?

2. Methods

2.1. Properties and Processes Regulating pCO_2

[7] The exchange of carbon between the ocean and atmosphere is given by $F = k\alpha\Delta pCO_2$, where F is the flux of CO_2; k is the CO_2 gas transfer velocity parameterized as a function of wind speed; α is the solubility of CO_2 in seawater; and ΔpCO_2 is the sea-air difference in the partial pressure of CO_2, determining the direction of flux. Because seawater pCO_2 in the surface mixed layer varies greatly in time and space relative to that in the atmosphere, it is the oceanic pCO_2 that predominantly regulates gas exchange [*Takahashi et al.*, 2002, 2009]. For this reason, we focus our study on processes controlling sea surface pCO_2 in the study region.

[8] The North Pacific carbon sink region exhibits a strong seasonal cycle in sea surface pCO_2, oscillating between relatively low pCO_2 in winter and high pCO_2 in summer. In the winter, the low sea surface pCO_2 creates an air-sea pCO_2 gradient favorable for oceanic uptake. This drives the region to absorb a large amount of atmospheric CO_2, an exchange enhanced by strong winter winds. In the high-pCO_2 summer months, the air-sea pCO_2 gradient relaxes and changes direction to a small extent, resulting in the region acting as a neutral to weak source for atmospheric CO_2. When considered on a mean annual basis, the large wintertime carbon uptake dominates and the net flux is into the ocean. In this manner, sea surface pCO_2 regulates air-sea CO_2 flux in the region.

[9] To understand the processes regulating sea surface pCO_2 in the North Pacific carbon sink region, we reconstruct the pCO_2 signal in the North Pacific from observational data.

Specifically, we use the thermodynamic relationship determined by *Takahashi et al.* [1993] to describe how pCO_2 changes with changes in temperature (T), salinity (S), dissolved inorganic carbon (DIC), and alkalinity (ALK):

$$\frac{\partial pCO_2}{\partial t} = \left(\frac{\partial pCO_2}{\partial T}\right)\frac{\partial T}{\partial t} + \left(\frac{\partial pCO_2}{\partial S}\right)\frac{\partial S}{\partial t} + \left(\frac{\partial pCO_2}{\partial DIC}\right)\frac{\partial DIC}{\partial t} + \left(\frac{\partial pCO_2}{\partial ALK}\right)\frac{\partial ALK}{\partial t}, \quad (1)$$

where the pCO_2 tendency terms are given by

$$\left(\frac{\partial pCO_2}{\partial T}\right) = (pCO_2)\left(0.0423^\circ C^{-1}\right), \quad (2)$$

$$\left(\frac{\partial pCO_2}{\partial S}\right) = \left(\frac{pCO_2 * \text{Salinity Factor}}{S}\right), \quad (3)$$

$$\left(\frac{\partial pCO_2}{\partial DIC}\right) = \left(\frac{pCO_2 * \text{Revelle Factor}}{\text{DIC}}\right), \quad (4)$$

$$\left(\frac{\partial pCO_2}{\partial ALK}\right) = \left(\frac{pCO_2 * \text{Alkalinity Factor}}{\text{ALK}}\right). \quad (5)$$

[10] The left-hand side (LHS) of equation (1) describes local changes in sea surface pCO_2 per unit time, resulting from local changes in the four properties on the right-hand side (RHS) of the equation. Because this governing equation describes how pCO_2 changes with changes in T, S, DIC and ALK, rather than the absolute value of pCO_2 as a function of the absolute values of T, S, DIC, and ALK, this work quantifies and discusses regulatory controls on changes in pCO_2 per unit time.

[11] As data for the local time rates of change of DIC and ALK found in equation (1) are not available, they are estimated using the following conservation equations:

$$\left.\frac{\partial DIC}{\partial t}\right|_{\text{MLD}}^{0} = -\nabla\cdot\mathbf{u}_{\text{HEk}}DIC - \nabla\cdot\mathbf{u}_{\text{Geo}}DIC - dwDIC/dz + k_H\nabla_H^2 DIC + k_V\left(\partial^2 DIC/\partial z^2\right) + dDIC_{\text{biology}} + dDIC_{\text{air-sea flux}} \quad (6)$$

$$\left.\frac{\partial ALK}{\partial t}\right|_{\text{MLD}}^{0} = -\nabla\cdot\mathbf{u}_{\text{HEk}}ALK - \nabla\cdot\mathbf{u}_{\text{Geo}}ALK - dwALK/dz + k_H\nabla_H^2 ALK + k_V\left(\partial^2 ALK/\partial z^2\right) + dALK_{\text{biology}}. \quad (7)$$

[12] Subscripts H and V indicate horizontal and vertical, respectively, describing either the eddy diffusion coefficient or the component of the velocity vector. The terms on the right-hand side of equations (6) and (7) indicate (1–3) the convergence of DIC and ALK due to horizontal Ekman (HEk), geostrophic (Geo), and vertical (w) advection, (4–5) the convergence of DIC and ALK due to horizontal and vertical mixing, (6–7) sources and sinks of DIC and ALK, due to biological processes and air-sea carbon flux (affecting DIC only).

[13] Though sea surface pCO_2 varies with changes in the seawater properties temperature, salinity, DIC, and ALK (equation (1)), it is perhaps more useful to think about changes in pCO_2 as a result of the processes that change those properties. Substituting equations (6) and (7) into equation (1) and regrouping terms yields the following rearrangement of processes regulating seawater pCO_2:

$$\frac{\partial pCO_2}{\partial t} = \partial pCO_{2\left(\begin{smallmatrix}\text{temperature}\\ \text{effects}\end{smallmatrix}\right)} + \partial pCO_{2\left(\begin{smallmatrix}\text{salinity}\\ \text{effects}\end{smallmatrix}\right)} + \partial pCO_{2\left(\begin{smallmatrix}\text{advection}\\ \text{of DIC and ALK}\end{smallmatrix}\right)} + \partial pCO_{2\left(\begin{smallmatrix}\text{mixing}\\ \text{of DIC and ALK}\end{smallmatrix}\right)} + \partial pCO_{2\left(\begin{smallmatrix}\text{biological impacts}\\ \text{on DIC and ALK}\end{smallmatrix}\right)} + \partial pCO_{2\left(\begin{smallmatrix}\text{air-sea flux}\\ \text{impacts on DIC}\end{smallmatrix}\right)}. \quad (8)$$

[14] Equation (8) states that pCO_2 in the surface mixed layer changes due to the six processes on the right-hand side of the equation: (1) temperature effects, (2) salinity effects, (3) advection, calculated as the change in pCO_2 resulting from the combined effects of the horizontal Ekman, geostrophic, and vertical convergences of DIC and ALK, (4) mixing, calculated as the change in pCO_2 resulting from the convergences of DIC and ALK due to horizontal and vertical mixing, (5) biological production and export, and (6) air-sea carbon flux. The remainder of this paper discusses changes in sea surface pCO_2 in terms of these six processes.

[15] The goal of this work, to understand processes regulating air-sea carbon flux in the North Pacific carbon sink region, can now be framed in terms of equation (8). On a seasonal basis, at any given location, seawater pCO_2 (LHS) increases and decreases as a result of the processes on the RHS: changes in temperature, changes in salinity, advection, mixing, biology, and air-sea flux. Quantifying the terms in equation (8) will reveal the dominant processes forcing this seasonal pCO_2 variability. On the other hand, seawater pCO_2 (LHS) shows no change on a mean annual basis, coming full circle over the course of a year at any given location. Yet, this region is known to be a strong annual sink for atmospheric CO_2 (a negative air-sea flux, by convention), represented by a positive value for term 6 on the RHS. This increase in pCO_2 (RHS term 6) must therefore be balanced by one or more of the other five terms on the RHS. Quantifying the terms of equation (8) will reveal which of these other processes decrease pCO_2 on an annual basis and to what extent, thus enabling the air-sea carbon flux into the ocean. Finally, on interannual timescales seawater pCO_2 (LHS) trends slowly upward as atmospheric CO_2 levels rise [*Takahashi et al.*, 2006]. We leave an investigation of controls on interannual seawater pCO_2 trends and variability to future studies.

[16] This work investigates controls on seawater pCO_2 in the North Pacific carbon sink region by quantifying the expected monthly climatological changes in pCO_2 due to its regulatory properties and processes. To the extent that these predicted changes in pCO_2 match the observed changes in pCO_2, they give us an understanding of processes regulating pCO_2 in this region. Details of our calculations follow.

Table 1. Data Sources

Parameter	Data Source	Spatial Resolution	Time Resolution
pCO_2, salinity, air-sea flux	*Takahashi et al.* [2010]	4°lat × 5°lon	data spanning 1970–2007, corrected to year 2000 by removing the interannual trend, and resolved monthly
DIC, ALK	GLODAP, *Key et al.* [2004] and *Sabine et al.* [2005]	1° × 1°	monthly, derived by averaging over the monthly climatological MLD; MLD data spans 1972–1999
Temperature	MODIS Aqua, available at http://modis.gsfc.nasa.gov/	9 km, regridded to 1° × 1°	monthly climatologies 2003–2010
Geostrophic velocity	produced by Ssalto/Duacs, distributed by Aviso with support from Cnes http://www.aviso.oceanobs.com/duacs/	1/3° × 1/3°, regridded to 1° × 1°	monthly climatologies 1993–2007
Wind speed	QuikSCAT, NASA PODAAC http://podaac.jpl.nasa.gov/	0.25° × 0.25°, regridded to 1° × 1°	monthly climatologies 2000–2008
Density	WOA05 (T,S) *Antonov et al.* [2006] and *Locarnini et al.* [2006]	1° × 1°	monthly climatologies through 2005
Primary productivity	*Behrenfeld and Falkowski* [1997] and *Westberry et al.* [2008]	1° × 1°	monthly climatologies 2003–2009, 1998–2007

2.2. Calculation Details

[17] Equation (1) (and thus equations (2)–(8)) is evaluated on a monthly basis over the monthly climatological mixed layer. Though studies investigating carbon dynamics sometimes consider the impact of processes on carbon chemistry within the upper 100 m by convention [*Sarmiento et al.*, 2002; *Ullman et al.*, 2009], here we choose to use the upper mixed layer based upon our research goals. To quantify the impact of processes forcing changes in sea surface pCO_2, assumed equivalent to mixed layer pCO_2 (equation (1), LHS), we also evaluate changes in T, S, DIC and ALK concentrations (equation (1), RHS) within the monthly climatological mixed layer volume. The mixed layer depth has a clear physical meaning that the 100 m depth horizon lacks, supporting this choice. The depth at which σ_θ increases by 0.125 from the surface value determines the base of the mixed layer, using World Ocean Atlas 2005 temperature and salinity data [*Locarnini et al.*, 2006; *Antonov et al.*, 2006].

[18] The uncertainty bounds for the predicted monthly changes in seawater pCO_2 (LHS, equations (1) and (8)) are estimated via propagating the errors from the individual terms on the RHS. Uncertainty bounds for the RHS terms are calculated via a Monte Carlo simulation, using the mean and probability distribution for each variable, or as appropriate, for the least known variable.

[19] As most data were available at spatial resolutions of 1° × 1° or finer, all calculations are done at this 1° × 1° scale. However, because seawater pCO_2 data is needed for each term in equation (1) but available only at a 4° latitude by 5° longitude resolution, all figures are presented on this coarser grid. Though figures show the entire North Pacific basin for context, the quantification of each term is reported as an average over our study area, the North Pacific carbon sink region as outlined in Figure 1. Sections 2.2.1–2.3 describe the calculation of each term in equation (1) (and thus equations (2)–(8)). Table 1 summarizes data sources used.

2.2.1. Observed Monthly pCO_2 Changes

[20] Observed changes in surface mixed layer pCO_2 are calculated on a monthly basis from the *Takahashi et al.* [2010] data set, a compilation of seawater pCO_2 and related measurements taken between 1970 and 2007, interpolated to a 4° latitude by 5° longitude grid, and corrected to a reference year 2000. This data reflects the expected seawater pCO_2 values in that reference year, calculated by removing the increasing trend in seawater pCO_2 in time, driven by increasing atmospheric CO_2 levels [*Takahashi et al.*, 2009]. The use of a linear trend to correct the data to a reference year introduced error in the observed pCO_2 values; we estimate this via a Monte Carlo simulation using an uncertainty envelope determined as follows. The mean annual rate of increase in pCO_2 in the North Pacific is approximately 1.2 μatm yr^{-1} in the open ocean, though spatially it varies between 0.5 and 2 μatm yr^{-1} [*Takahashi et al.*, 2009]. This rate is slower than the global mean rate of increase of 1.5 μatm yr^{-1} that was used to time-adjust the data set [*Takahashi et al.*, 2009]. This difference, about 0.3 μatm yr^{-1}, multiplied by the length of time that an average pCO_2 measurement might need to be adjusted upward, (2000–1970)/2 = 15 years, yields a lower uncertainty bound of −4.5 μatm. Similarly, 0.3 μatm yr^{-1} multiplied by (2007–2000)/2 = 3.5 years gives an upper uncertainty bound of +1.0 μatm for the Monte Carlo simulation. Though the observational pCO_2 data represents the year 2000, monthly climatological data are used for all other variables in this study.

2.2.2. Predicted Monthly pCO_2 Changes

[21] Predicted changes in seawater pCO_2 are estimated on a monthly basis according to equation (1). The LHS of equation (1) indicates predicted changes in pCO_2, calculated as the sum of the four terms on the RHS of the equation. The terms on the RHS each contain two parts: a pCO_2 dependency term, describing how pCO_2 changes with changes in a given seawater property, and a time rate of change term for each property. Sections 2.2.3 and 2.2.4 describe the calculation of these RHS terms.

2.2.3. Dependency of pCO_2 on T, S, DIC, and ALK

[22] The four pCO_2 dependency terms on the RHS of equation (1) are calculated according to equations (2)–(5). The Revelle Factor and Alkalinity Factor are calculated using the CO2SYS carbon chemistry program [*van Heuven et al.*, 2009], with the Mehrbach dissociation constants refit

by Dickson and Millero [*Dickson and Millero*, 1987]. As the Revelle Factor and Alkalinity Factor are close in value but opposite in sign, changes in DIC and ALK effect a similar magnitude of change in pCO_2, but in opposing directions [*Takahashi et al.*, 1993]. For the Salinity Factor we use 1.6 [*Sarmiento and Gruber*, 2006], rather than the 0.94 given by *Takahashi et al.* [1993]. This accounts for dilution effects on carbon chemistry due to freshening, in addition to the direct effect of salinity on the carbon system dissociation constants. Use of such a global approximation is appropriate, as the impact of salinity on pCO_2 is small relative to other factors.

2.2.4. Time Rate of Change of T, S, DIC, and ALK

[23] The four time rate of change terms on the RHS of equation (1) are calculated as follows. The local time rate of change of temperature (RHS, term 1) is calculated using monthly climatological sea surface temperature data (2003–2010) from the MODIS sensor on NASA's Aqua satellite. Uncertainty is represented as one standard deviation of the interannual variability in local sea surface temperature. The local time rate of change of salinity (RHS, term 2) is calculated from the *Takahashi et al.* [2010] data set. As salinity plays a negligible role in carbon dynamics relative to other factors in this region, uncertainty was not estimated.

[24] The local time rates of change of DIC and ALK (RHS, terms 3 and 4) are calculated according to the conservation equations (6) and (7). DIC and ALK data, used in calculating terms 1–5 on the RHS of equations (6) and (7), are from the Global Ocean Data Analysis Project (GLODAP) data set [*Key et al.*, 2004; *Sabine et al.*, 2005]. Though DIC and ALK are often normalized to a constant salinity by convention to remove the effects of evaporation and dilution [*Dore et al.*, 2003], normalizing in space does not make sense for our large study area with strong spatial gradients in salinity, and it is not clear that there is a benefit to removing the seasonal salinity signal by normalizing in time. We calculate equation (1) both ways, using DIC and ALK data salinity-normalized in time, as well as nonnormalized DIC and ALK data, and find that salinity normalization makes little difference to the reconstructed pCO_2 signal (as will be shown in section 2.4). Therefore we choose to carry the nonnormalized calculations through the rest of the study.

[25] The GLODAP data set used for DIC and ALK is a synthesis of ocean carbon measurements taken between 1972 and 1999 and interpolated to a single $1° \times 1°$ horizontal grid at selected depths, representing an annual climatology [*Key et al.*, 2004; *Sabine et al.*, 2005]. Time series of observational carbon data exist, but only for relatively few mooring sites. Seasonal variations of DIC and ALK have been approximated globally by regressing them with T, S, and biologically mediated quantities such as nitrate [*Lee*, 2001], and below the deepest winter mixed layer depths only, apparent oxygen utilization rate [*Goyet et al.*, 2000]. However, we seek mixed layer values, and because regressing DIC and ALK with nitrate may introduce large regional errors, particularly in subtropical waters with potentially significant rates of nitrogen fixation [*Karl et al.*, 1997], here we choose a simpler approach.

[26] We derive annual cycles of DIC and ALK by averaging monthly over the climatological mixed layer depth. The resulting derived annual cycle of DIC has an average seasonal amplitude of 33 μmol kg^{-1} in the North Pacific carbon sink region (our study region, as outlined in Figure 1), with minima in July/August and maxima in February/March. Available literature values suggest this is a reasonable approximation of the region's seasonal cycle. South of our study region, at station ALOHA (22°45′N, 150°W), *Emerson et al.* [1997] found the seasonal amplitude of DIC to be ~16 and 19 μmol kg^{-1} in each of two years, also with minima in July/August and maxima in February/March; in this same location our derived annual cycle of DIC shows a similar seasonal amplitude of 21 μmol kg^{-1}. The lesser seasonal amplitude of DIC at station ALOHA as compared to the our study region is consistent with our expectation that the transition zone have a more pronounced seasonal cycle than the rest of the subtropical gyre, due to greater seasonal differences in primary productivity and mixing depths. In the western portion of our study region (approximately 35–42°N and 140–160°E, the region off southeast Japan in the Kuroshio), 2 years of ship data showed mixed layer DIC to vary seasonally by ~100 μmol kg^{-1}, with minima and maxima around July and February [*Wong et al.*, 2002a, 2002b]. In this same region, our derived annual DIC cycle shows a seasonal amplitude of 77 μmol kg^{-1}, also with a minimum in July and a maximum in February. North of our study region, at station KNOT (44°N, 155°E), our derived seasonal DIC cycle has a range of 70 μmol kg^{-1}, as compared to the ~100 μmol kg^{-1} reported by *Tsurushima et al.* [2002]. Our apparent underestimation of the DIC amplitude by ~25% in the west and to the north of our study region is likely an upper bound for the carbon sink region as a whole, as this dynamic portion of the basin has the largest seasonal fluctuations [*Wong et al.*, 2002b]. While our derived DIC and ALK cycles capture the majority of seasonal variability, we acknowledge that associated error remains. Because the GLODAP data is summer biased [*Key et al.*, 2004], we expect the apparent underestimation of the seasonal DIC amplitude remaining to result in too low fall and winter DIC values, rather than too high spring and summer DIC values. We will return to this in section 3. Our calculations for the time rate of the change of DIC and ALK (equations (6) and (7)) are outlined term by term as follows in the rest of section 2.

2.2.4.1. Advection of DIC and ALK

[27] For term 1 (RHS), the horizontal Ekman convergences of DIC and ALK are calculated as $-\nabla \cdot \mathbf{u}_{HEk}\overline{DIC}$ and $-\nabla \cdot \mathbf{u}_{HEk}\overline{ALK}$, where $\mathbf{u}_{HEk}$ is the horizontal Ekman velocity and $\overline{DIC}$ and $\overline{ALK}$ are the average DIC and ALK concentrations in the mixed layer, assumed to be the same as those in the generally shallower Ekman layer depth. This gain or loss of DIC or ALK from the convergence or divergence of Ekman fluxes is distributed throughout the mixed layer to yield the change in mixed layer DIC and ALK concentrations due to horizontal Ekman flow. Monthly climatological horizontal Ekman velocities are calculated as $u_{HEk} = \tau_y/\rho f D$ and $v_{HEk} = \tau_x/\rho f D$, where τ is the wind stress, ρ is density, f is the Coriolis parameter, and D is the Ekman depth. Wind velocity data are from the QuikSCAT scatterometer, distributed by the NASA Physical Oceanography Distributed Active Archive Center (PODAAC). Uncertainty estimated using a Monte Carlo simulation takes the standard deviations of the Ekman transports to be 25% of the mean [*Stoll et al.*, 1996].

[28] For term 2, the geostrophic convergences of mixed layer DIC and ALK are calculated as $-\nabla \cdot \mathbf{u}_{Geo}\overline{DIC}$ and $-\nabla \cdot \mathbf{u}_{Geo}\overline{ALK}$, where $\mathbf{u}_{Geo}$ is the monthly climatological geostrophic velocity. Geostrophic velocity data are assumed constant throughout the mixed layer. Uncertainty estimated with a Monte Carlo simulation takes the standard deviations of geostrophic currents in the Kuroshio region to be 22% of the mean [*Kakinoki et al.*, 2008].

[29] For term 3, convergences of DIC and ALK in the mixed layer due to vertical advection are calculated as $-w(\Delta DIC)/MLD$ and $-w(\Delta ALK)/MLD$, where $\Delta DIC = DIC_{@MLD+\Delta Z} - \overline{DIC}$, $\Delta ALK = ALK_{@MLD+\Delta Z} - \overline{ALK}$, and ΔZ is 25 m. While the vertical velocity is zero at the surface, the vertical velocity at the base of the mixed layer can be written as $w = \partial MLD/\partial t + \nabla_H \cdot \mathbf{v}_H MLD$ where $\mathbf{v}_H$ is the vertically averaged horizontal velocity of the mixed layer [*Stevenson and Niiler*, 1983; *Swenson and Hansen*, 1999]. The two processes on the RHS contributing to this vertical velocity are: local changes in the mixed layer depth due to wind mixing and/or buoyancy forcing, and vertical velocity that results from a convergence or divergence in the horizontal thickness flux. Of these, the local change in mixed layer depth dominates the vertical velocity, and thus also dominates the vertical convergence of DIC and ALK. As the mixed layer deepens, DIC and ALK-rich deep waters are entrained into upper waters; as the mixed layer shoals, ΔDIC and ΔALK are zero, leaving DIC and ALK concentrations in the mixed layer unchanged.

2.2.4.2. Mixing of DIC and ALK

[30] For term 4, the convergences of DIC and ALK due to horizontal mixing are estimated as $k_H(\Delta\overline{DIC}/\Delta X^2 + \Delta\overline{DIC}/\Delta Y^2)$ and $k_H(\Delta\overline{ALK}/\Delta X^2 + \Delta\overline{ALK}/\Delta Y^2)$. As the greatest uncertainty in the calculation of these terms lies in the uncertainty of the eddy diffusivity coefficient, k_H, we use a high and low estimate to bound its probability distribution for the Monte Carlo simulation. The low estimate, k_H = 500 $m^2\ s^{-1}$, is listed by *Visbeck et al.* [1997] for the Ekman convergence zone of the North Pacific; the high estimate, $k_H = 2 \times 10^3\ m^2\ s^{-1}$, is given by *Kimura et al.* [1997] for the Kuroshio region.

[31] For term 5, the convergences of DIC and ALK due to vertical mixing are evaluated as $k_V(DIC_{@MLD+\Delta Z} - \overline{DIC})/\Delta Z^2$ and $k_V(ALK_{@MLD+\Delta Z} - \overline{ALK})/\Delta Z^2$, where ΔZ is again 25 m. This convergence is distributed throughout the mixed layer to yield the change in mixed layer DIC and ALK concentrations due to vertical mixing across the base. The vertical diffusivity coefficient, k_V, introduces the largest source of uncertainty. Localized estimates of k_V range from $10^{-5}\ m^2\ s^{-1}$ to $10^{-4}\ m^2\ s^{-1}$, and are on the order of $3 \times 10^{-5}\ m^2\ s^{-1}$ averaged over the global oceans [*Webb and Suginohara*, 2001]. *Kimura et al.* [2000] suggest a k_V of $10^{-4}\ m^2\ s^{-1}$ for the Kuroshio Extension region, a region of intensified local mixing. Here we use a mean k_V of $10^{-4} \pm 5 \times 10^{-5}\ m^2\ s^{-1}$ in the Kuroshio extension region, and a k_V of $3 \pm 5 \times 10^{-5}\ m^2\ s^{-1}$ elsewhere.

2.2.4.3. Sources and Sinks of DIC and ALK

[32] For term 6, estimates of biological changes in DIC and ALK are addressed in section 2.3, to allow for a more thorough discussion.

[33] For term 7, the time rate of change of DIC due to air-sea gas exchange is calculated monthly by distributing the *Takahashi et al.* [2010] air-sea CO_2 flux per unit area into the mixed layer. The air-sea CO_2 flux uncertainty used in the Monte Carlo simulation is ± 53%, as suggested by *Takahashi et al.* [2009].

2.3. Biological Drawdown

[34] Biological drawdown of pCO_2 is one of the dominant, yet least-constrained processes regulating air-sea carbon flux [*Takahashi et al.*, 1993; *Emerson et al.*, 1997]. Quantifying the biological pump is difficult; even at mooring sites such as station ALOHA in the subtropical North Pacific, *Emerson et al.* [1997] estimated the uncertainty of the biological pump to be ± 50%. As quantifying biological impacts on pCO_2 remains essential to understanding air-sea flux, we estimate it along with appropriate measures of uncertainty.

[35] Biological activity affects sea surface pCO_2 through its impact on both DIC and ALK in upper waters. Biological production impacts DIC primarily via the export of organic matter to depth: one mole of organic carbon exported lowers DIC by one mole [*Zeebe and Wolf-Gladrow*, 2001]. Biological production secondarily affects DIC and ALK in surface waters by the formation and sinking of $CaCO_3$: one mole of $CaCO_3$ exported lowers DIC by one mole and ALK by two [*Zeebe and Wolf-Gladrow*, 2001]. Finally, biological production also affects ALK by the uptake of nitrate to form organic matter, a process which uses hydrogen ions and thus raises ALK [*Brewer et al.*, 1975]. We estimate these biological impacts on DIC and ALK in surface waters as described in sections 2.3.1–2.3.3.

2.3.1. Organic Carbon Export

[36] We estimate the total organic carbon exported from surface waters, which can be in the form of either particulate organic carbon (POC) or dissolved organic carbon (DOC) [*Ogawa and Tanoue*, 2003], as a fraction of net primary production (NPP). First, we estimate column-integrated NPP (mol C m^2 $month^{-1}$), defined as photosynthesis minus autotrophic respiration, via two satellite data-based global models. The Vertically Generalized Production Model (VGPM) of *Behrenfeld and Falkowski* [1997], based on chlorophyll measurements, yields one estimate of net primary productivity. The vertically resolved Carbon-based Production Model (CbPM2) of *Westberry et al.* [2008], yields a second. This NPP minus heterotrophic respiration is the net community production (NCP), which in steady state, is equivalent to the organic carbon exported from surface waters.

[37] Next, we assume steady state and estimate organic carbon export from the above NPP estimates using three different export ratios. First, we apply the primarily temperature and chlorophyll-based POC export ratio of *Dunne et al.* [2005] to our two estimates of net productivity above. As the *Dunne et al.* [2005] export estimate does not include DOC, we increase it based on the approximation that globally, DOC export comprises about 20% of total organic carbon flux to the deep ocean [*Carlson et al.*, 1994; *Hopkinson and Vallino*, 2005]. Second, we apply the temperature-dominated export ratio algorithm of *Laws et al.* [2000], which already includes both DOC and POC, to our net primary productivity estimates. And third, we apply the notably higher export ratio of 0.36 ± 0.23, determined for the North Pacific transition zone by *Juranek* [2007] from triple oxygen isotopes and O_2/Ar ratios, to arrive at NCP,

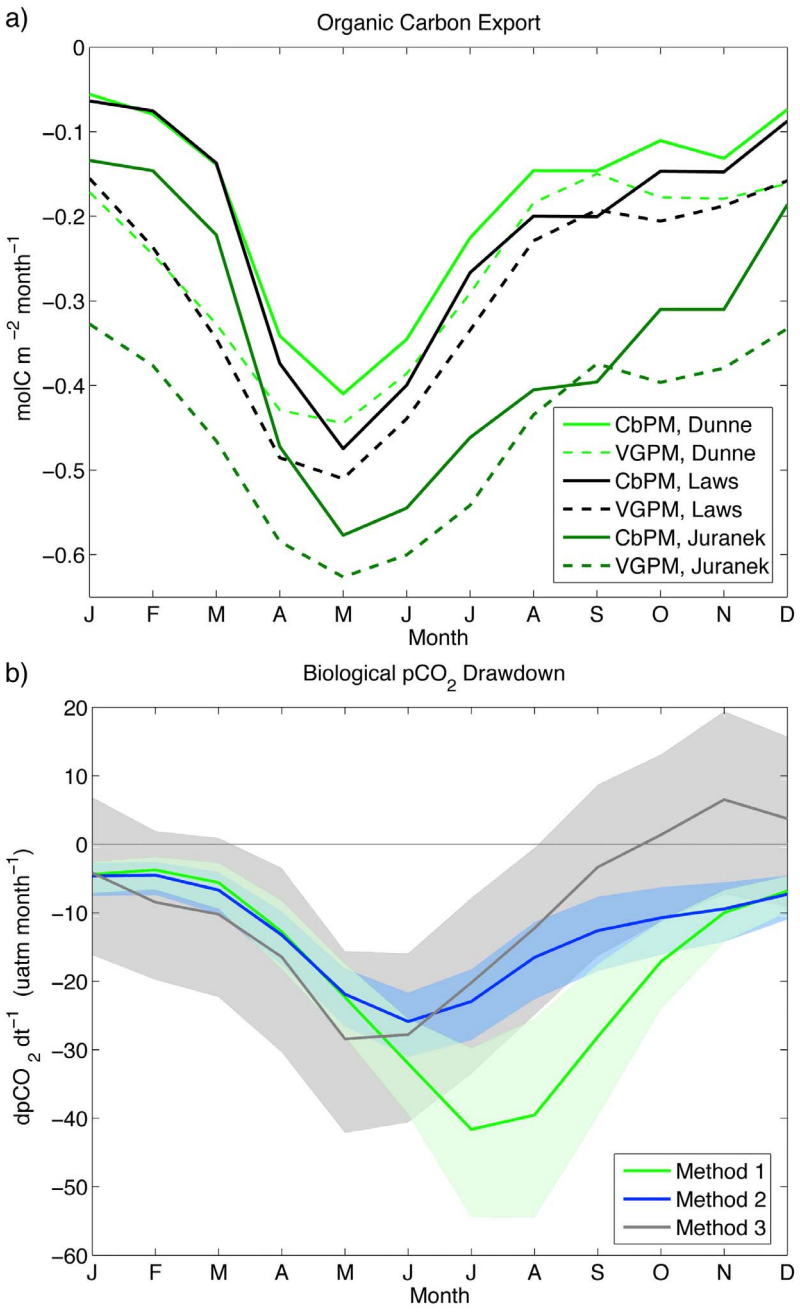

Figure 2. (a) Six different estimates of organic carbon export, derived from VGPM (dashed) and CbPM (solid) net primary productivity estimates in conjunction with Dunne, Laws, and Juranek export ratios. (b) Corresponding mean monthly biological pCO_2 drawdown, estimated three ways: (1) due to biological impacts on DIC and ALK in the MLD (green), (2) due to biological impacts on DIC and ALK in the surface 20 m (blue), and (3) by determining what the biological drawdown on pCO_2 would have to be, if the estimated monthly changes due to all other processes were accurate (gray). Solid lines indicate the mean; shading indicates 1 standard deviation. All values are averaged over the study area outlined in Figure 1.

equivalent to export production in steady state. In this manner, using two estimates of NPP and three different export ratios, we arrive at six estimates of organic carbon export.

[38] These six different estimates of column-integrated organic carbon export are shown in Figure 2a, averaged monthly and spatially over our study domain. Overall, they are remarkably similar. The VGPM predicts slightly higher drawdown in this region than the CbPM2. The export production calculated using the *Juranek* [2007] export ratio, which is based on *in situ* data in the region but biased toward high-productivity months, is larger than that calculated using either the *Laws et al.* [2000] or *Dunne et al.* [2005] export ratios, each of which are global algorithms. Given the uncertainty associated with both the production models and export ratios, we choose to use the mean of these six

different export estimates, and represent uncertainty as one standard deviation. Our biological export estimates calculated in this manner are consistent with *in situ* data available. *Howard et al.* [2010] report net community productivity values from O_2/Ar ratios in the North Pacific transition zone from September 2008 as 8.1 ± 2.7 mmol C m^{-2} d^{-1} (0.24 ± 0.08 mol C m^{-2} $month^{-1}$) and November 1997 as 3.4 ± 2.0 mmol C m^{-2} d^{-1} (0.1 ± 0.06 mol C m^{-2} $month^{-1}$). These values are indistinguishable from our climatological monthly estimates in the region, at 0.19 ± 0.06 mol C m^{-2} $month^{-1}$ for September, and 0.18 ± 0.05 mol C m^{-2} $month^{-1}$ for November. Our annual biological carbon drawdown estimate of 3.1 ± 0.35 mol C m^{-2} yr^{-1} for the North Pacific carbon sink region is also broadly consistent with *in situ* observations at other sites in the North Pacific, from 2.6 ± 0.9 mol C m^{-2} yr^{-1} in the subtropical Pacific at station ALOHA to 2.0 ± 0.5 mol C m^{-2} yr^{-1} in the subarctic Pacific at station P [*Emerson and Stump*, 2010]. Thus our estimates of organic carbon export are consistent with literature values.

2.3.2. $CaCO_3$ Precipitation

[39] Biological production additionally affects DIC and ALK in surface waters via the formation and precipitation of $CaCO_3$, which we estimate as proportional to POC export. Literature values for the global $CaCO_3$:POC ratio (also called the rain rate) include: 0.05–0.08 [*Milliman and Troy*, 1999], 0.10–0.12 [*Lee*, 2001], and 0.08 [*Yamanaka and Tajika*, 1996], corrected to ~0.09 by *Sarmiento et al.* [2002]. *Sarmiento et al.* [2002] estimate the global rain rate at 0.06 ± 0.03 and the North Pacific subtropical gyre (15°–45°N) rain rate at 0.048 ± 0.011. They note that their methods trend toward underestimation in subtropical waters, which would include our dynamically subtropical study area [*Ayers and Lozier*, 2010]. Though rain rate estimates in our study region in the North Pacific transition zone are unavailable, literature estimates in the subarctic Pacific range from 0.10 at station KNOT (44°N, 155°E) [*Noriki et al.*, 1999] to 0.35 [*Wong et al.*, 2002c] and 0.5 [*Emerson et al.*, 2011] at ocean station P (OSP) (50°N, 145°W). We expect OSP, because it is in the highly calcifying eastern subarctic [*Wong et al.*, 2002c], to have higher $CaCO_3$:POC ratios than our region. Because for our region the OSP rain rates are expected to be overestimates, and the Sarmiento rates expected to be underestimates, in this study we estimate $CaCO_3$ precipitation using an intermediate $CaCO_3$:POC ratio of 0.1, a choice broadly supported in the literature.

2.3.3. Nitrate Uptake

[40] Biological production also affects alkalinity in surface waters via the utilization of nitrate (NO_3^-). The uptake of one mol of NO_3^-, accompanied by the parallel uptake of one mol of hydrogen ions, H^+, increases alkalinity by one mol [*Brewer et al.*, 1975; *Brewer and Goldman*, 1976; *Goldman and Brewer*, 1980]. Here we estimate nitrate uptake from our NPP estimates using 16N:106C Redfield stoichiometry. The increase in alkalinity due to biological nitrogen utilization opposes its decrease due to $CaCO_3$ precipitation.

[41] The sum of these biological changes in DIC and ALK due to organic carbon export, $CaCO_3$ precipitation, and nitrate utilization are represented in equations (6) and (7), RHS terms 6. The impact of these biological changes in DIC and ALK on seawater pCO_2 is considered next.

2.3.4. Drawdown of pCO_2

[42] Biological changes in DIC and ALK affect air-sea gas exchange through their corresponding impact on pCO_2 in surface waters; however, as biological changes in DIC and ALK occur throughout the water column, the depth over which they affect sea surface pCO_2 requires some consideration. We consider two possibilities. First, that seawater pCO_2 in upper waters changes as a function of biological changes in mixed layer DIC and ALK concentrations. Assuming carbon chemistry is homogenous within the mixed layer, changes in mixed layer DIC and ALK concentrations would be reflected at the surface. This approach is consistent with conservation equations (6) and (7) as written, and therefore our treatment of changes in DIC and ALK due to physical processes above. The biological drawdown of pCO_2 calculated in this manner is shown in Figure 2b (method 1, green). Though column-integrated export productivity peaks in May (Figure 2a), this method yields the greatest biological pCO_2 drawdown in July, when changes in DIC and ALK are distributed over the smallest mixed layer volume. In this way physics exerts control on the air-sea flux even during the high-productivity summer months: regardless of the timing of peak biological productivity, the largest pCO_2 drawdown occurs in months when the surface water is most stratified, and consequently, the biological export of DIC and ALK is most concentrated.

[43] Second, we consider the impact of biology on DIC and ALK concentrations over a fixed depth horizon. Because biological productivity rates, dependent on light penetration through the water column, are not homogenous within the mixed layer, we consider the impact of biology on DIC and ALK concentrations over a depth for which biological production rates are constant. This case assumes that biological production alters surface water chemistry, and consequently impacts pCO_2 and gas exchange, faster than mixing can homogenize it. In this case we consider biological impacts on DIC and ALK in the upper 20 m, based on the depth-resolved productivity estimates of *Westberry et al.* [2008], which estimate constant production rates from the surface to this depth in all months in our study region. Results would be the same for any shallower depth chosen. Figure 2b shows the biological drawdown of pCO_2 calculated in this manner (method 2, blue). This method shows the largest biological impact on sea surface pCO_2 to be May through July, closer to the May peak in total column-integrated production.

[44] Finally, we estimate biological impacts on pCO_2 via a third method, using equation (8): given our estimates of all other processes affecting pCO_2 (RHS terms 1–4 and 6), we solve for the biological drawdown needed (RHS term 5) to yield the observed pCO_2 (LHS). In this case the peak biological impact on pCO_2 is in May (Figure 2b, method 3, gray). We note that the increase in pCO_2 seen in autumn with this method is spurious, an artifact of underestimates of increases in pCO_2 due to other processes in this season. Drawdown estimates from this method are presented for comparison, rather than use throughout the rest of the study, because they are not independent from our quantification of other terms.

[45] Calculations throughout the rest of this paper use the mixed layer depth biological drawdown estimates from method 1, chosen for consistency. We note that regardless of

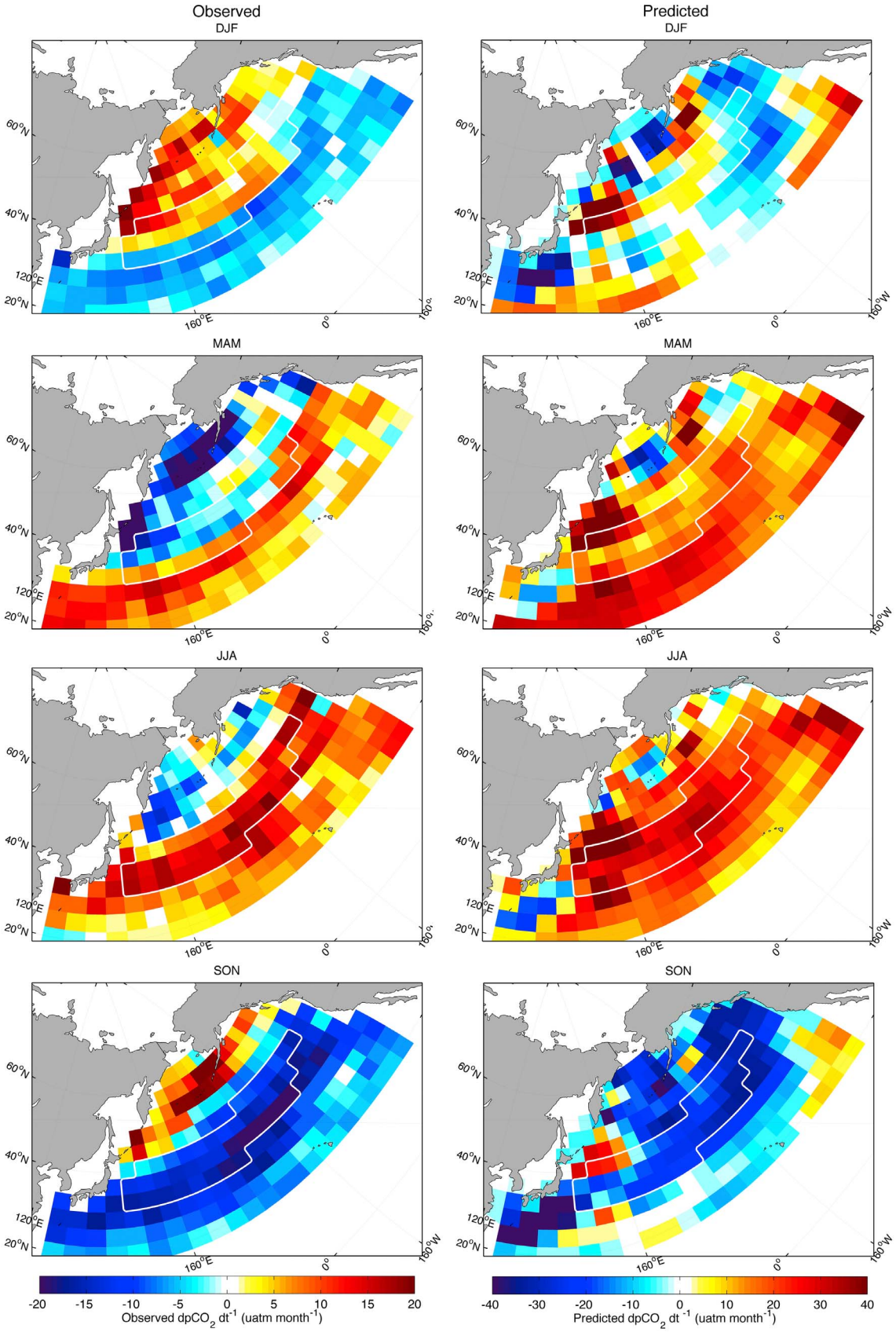

Figure 3. (left) Observed and (right) estimated changes in pCO_2 (μatm month^{-1}) in four seasons. Note the difference in color scales. Estimated pCO_2 changes successfully reconstruct the general spatial pattern and seasonality of the gyres. White outline indicates the study domain, as in Figure 1.

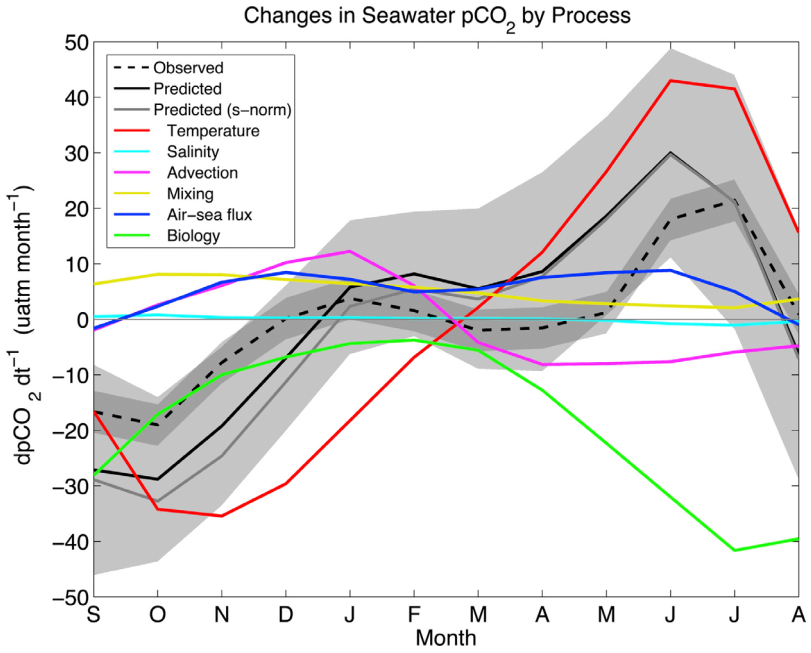

Figure 4. Processes regulating sea surface pCO_2 in the North Pacific carbon sink region. All values are averaged over the study region outlined in Figure 1. Observed monthly changes in pCO_2 (black dashed) are reasonably well approximated by predicted changes in pCO_2 (black solid). The predicted changes in pCO_2 calculated using salinity-normalized DIC and ALK data (gray solid) are negligibly different from those calculated without salinity normalizing (black solid). Predicted changes are calculated as the sum of changes due to the effects of temperature (red), salinity (cyan), advection (magenta), mixing (yellow), air-sea flux (blue), and biology (green). Uncertainty in $dpCO_2\ dt^{-1}$ due to individual processes is shown collectively in gray shading around the predicted curve. Darker gray shading indicates uncertainty in the observed $dpCO_2\ dt^{-1}$.

whether drawdown estimates from method 1 or method 2 are used, our results are robust: conclusions presented herein as to which processes regulate pCO_2 seasonally, annually, and determine the location of the sink remain unchanged.

2.4. Validation

[46] To the extent that our reconstructed changes in pCO_2 (equations (1) and (8), LHS) match observed changes in pCO_2, we can use these estimates to investigate processes regulating sea surface pCO_2 on seasonal to annual timescales. Figures 3 and 4 compare our pCO_2 estimates to the observational data, showing that estimated pCO_2 successfully reconstructs the seasonality of the North Pacific basin as well as the spatial pattern of the gyres. Seasonal pCO_2 dynamics in the subtropical and subpolar gyres have been generalized in terms of temperature and DIC controls on pCO_2 [*Takahashi et al.*, 1993, 2002]. These controls are manifest in Figure 3. In winter (DJF), the seasonal cooling of subtropical waters decreases seawater pCO_2 in this gyre, while increased upwelling and mixing of DIC-rich deep waters increase pCO_2 in the subpolar gyre. Come spring (MAM) and summer (JJA), the warming of subtropical waters increases pCO_2, while biological blooms in the no longer light-limited subpolar regions decrease pCO_2 in surface waters. In fall (SON), cooling of subtropical waters once again decreases pCO_2, while in the subpolar regions increased input of DIC-rich deep waters to the surface mixed layer once again increases pCO_2.

[47] The spatial pattern of the gyres (Figure 3) would be better reconstructed by our estimated pCO_2 changes if not for an overestimate of drawdown at high latitudes, particularly in the winter months, and an underestimate at low latitudes. This results from a N–S gradient in our biological carbon drawdown estimates derived from satellite-based primary productivity and export ratio algorithms. While such a gradient in annual export productivity has been widely accepted based on satellite data-based algorithms, increasingly available *in situ* observations have found no support for this [*Emerson and Stump*, 2010]. It is worth noting that our estimate of biological export derived not from satellite-based productivity algorithms, but deductively from our estimates of all other controls on pCO_2 (method 3), exhibited no N–S gradient in export production (not shown). This lends support that our quantification of all other controls on pCO_2 is reasonable. While the N–S uncertainty in biological pCO_2 drawdown impacts basin-scale spatial patterns, it has little effect on reconstructed pCO_2 changes in our region of interest, where the export productivity estimates match *in situ* observations well (shown previously in section 2.3.1).

[48] While Figure 3 shows reconstructed changes in pCO_2 basin-wide to verify the broad-scale spatial integrity of these estimates, our primary goal is to understand the pCO_2 signal in the North Pacific carbon sink region, as outlined in Figure 1. To that aim, our estimates have used parameters specific to the area: the vertical and horizontal mixing

Table 2. Observed and Estimated Changes in pCO_2 in Our Study Area, the North Pacific Carbon Sink Region as Outlined in Figure 1[a]

	SON (μatm month^{-1})	DJF (μatm month^{-1})	MAM (μatm month^{-1})	JJA (μatm month^{-1})	Mean Annual (μatm yr^{-1})
Observed	−14(±4)	2(±4)	−1(±4)	13(±4)	0(±24)
Estimated	−25(±9)	2(±7)	11(±10)	15(±13)	9(±64)
Temperature	−29(±6)	−18(±5)	13(±6)	33(±6)	0(±36)
Salinity	1	0	0	−1	0
Advection					
H. Ekman	4(±1)	3(±0)	2(±0)	3(±1)	32(±3)
Geostrophic	−9(±1)	−9(±1)	−10(±1)	−9(±1)	−113(±8)
Vertical	8(±1)	16(±1)	2(±0)	0(±0)	79(±5)
Mixing					
Horizontal	2(±1)	2(±1)	2(±1)	2(±1)	25(±4)
Vertical	6(±3)	4(±3)	1(±1)	1(±1)	36(±13)
Air-sea flux	2(±2)	7(±2)	7(±5)	4(±3)	61(±23)
Biology					
Method 1, MLD	−9(±5)	−2(±1)	−7(±4)	−19(±10)	−111(±36)
Method 2, 20 m	−7(±3)	−4(±2)	−8(±4)	−11(±5)	−88(±21)
Method 3	2(±8)	−3(±7)	−18(±9)	−20(±8)	−119(±51)

[a]Estimated changes in pCO_2 are calculated according to equation (8) as the sum of changes due to temperature effects, salinity effects, advection of DIC and ALK, mixing of DIC and ALK, air-sea flux, and biological processes. Error bounds indicate one standard deviation of the variability. Here pCO_2 is in units of μatm time^{-1}.

coefficients, the export production ratio given by *Juranek* [2007], and the calcium carbonate to particulate organic carbon export ratio. Larger deviations from observed values are thus expected outside of this region. Our reconstructed changes in pCO_2 indeed do best in our study region, with the normalized root mean square error (NRMSE) for annual mean changes in pCO_2 at 22%.

[49] Figure 4 shows that within our study region, our reconstructed changes in pCO_2 capture the basic timing and shape of the observed seasonal cycle (whether calculated using salinity-normalized DIC and ALK or not). Within this region, our reconstructed pCO_2 dynamics compare favorably with those generated by large-scale models. *McKinley et al.* [2006] evaluated the seasonal cycles of pCO_2 in seven different biogeochemical ocean models, and compared them to the observed pCO_2 cycles at three sites in the North Pacific: OSP (50°N, 145°W), in the Oyashio near the Kuril islands (46–50°N, 150–160°E), and station ALOHA (22°45′N, 158°W). In the dynamically complex Kuril region, all but one of the models failed to capture the basic seasonal cycle of pCO_2. At OSP and ALOHA the models did better, recreating the general shape of the seasonal cycle. At OSP the modeled $dpCO_2\ dt^{-1}$ for all models was within $\pm$ 25 μatm month^{-1} of the observed $dpCO_2\ dt^{-1}$. Within our study area of the North Pacific carbon sink region, our reconstructed $dpCO_2\ dt^{-1}$ captures the seasonal cycle to within $\pm$ 18 μatm month^{-1} of the observed. Though we capture the shape, the amplitude of our reconstructed pCO_2 seasonal cycle is somewhat too large compared to the observed. As the seasonal cycle of pCO_2 due to temperature effects is relatively known, this indicates an underestimation of the amplitude of the seasonal cycle due to all non-temperature effects, a problem common to many models [*McKinley et al.*, 2006]. As our reconstructed pCO_2 recreates the general shape and amplitude of the observed seasonal cycle by capturing the fundamental relationships among the processes impacting seawater pCO_2, similarly to *McKinley et al.* [2006], we conclude that our pCO_2 cycle is an adequate tool for investigating our questions of interest.

[50] Despite sources of uncertainty, our estimated changes in pCO_2 reconstruct observed changes in pCO_2 in the North Pacific carbon sink region remarkably well. Thus, this approach enables us to identify and quantify the impacts of processes regulating sea surface pCO_2 in this region on a seasonal (section 3) and mean annual basis (section 4). With this knowledge, we can then answer in section 5: why is the sink located where it is, and how do these waters maintain low sea surface pCO_2 and thus net atmospheric carbon uptake year after year?

3. Seasonal Controls on pCO_2

[51] As previously mentioned, the North Pacific transition zone region is a net sink for atmospheric carbon dioxide on an annual basis, but varies seasonally between a strong sink in winter and a neutral to weak source in summer. Equipped now with monthly estimates of pCO_2 changes due to each of its six regulatory processes (equation (8)), we investigate how these processes drive the seasonal pCO_2 cycle. While seasonal carbon dynamics have been described in the literature, we contribute a quantification of these processes.

[52] Predicted and observed monthly changes in pCO_2 are shown averaged over the study domain in Figure 4. The predicted monthly changes in seawater pCO_2 (solid black line) match the observed monthly changes (black dashed line) reasonably well, with both showing the distinct seasonal cycle. During fall and winter the sea surface pCO_2 generally decreases, creating a larger air-sea pCO_2 gradient favorable for oceanic uptake of CO_2. In spring and summer, the pCO_2 generally increases, decreasing the air-sea pCO_2 gradient and even reversing it slightly, driving the waters to become neutral to a weak source of atmospheric CO_2. This seasonal cycle is determined by how the six processes regulating pCO_2 on the RHS of equation (8) balance. The contribution of each of these processes to the seasonal pCO_2 cycle, shown graphically in Figure 4, is also summarized in Table 2.

[53] In the study region, temperature effects, shown in red, clearly dominate the seasonal pCO_2 cycle. In the spring and summer, the warming of waters increases sea surface pCO_2; in the fall and winter this effect is reversed as the cooling of waters drives a corresponding decrease in sea surface pCO_2.

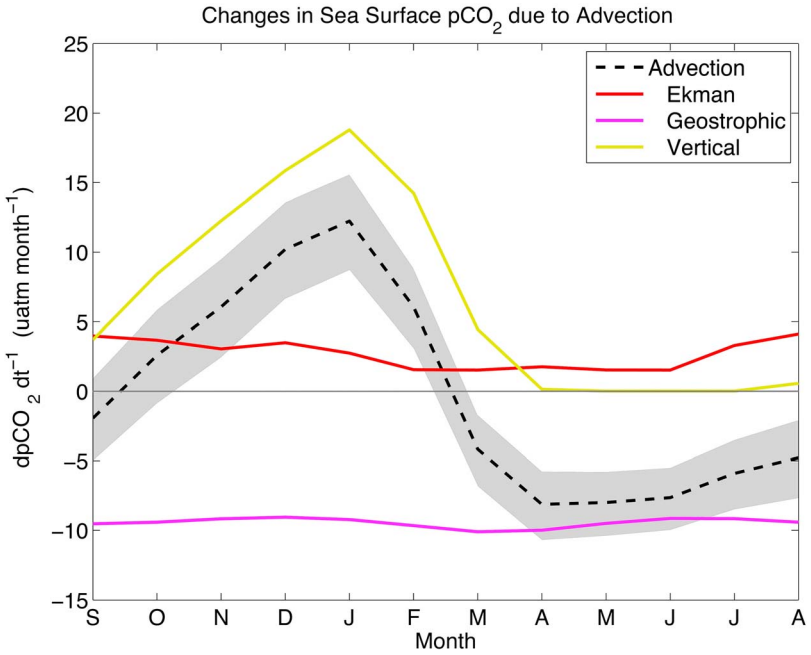

Figure 5. Change in mixed layer pCO_2 due to advection (black dashed line, equivalent to the magenta line in Figure 4), calculated as the sum of the change in pCO_2 due to the vertical (yellow), horizontal Ekman (red), and geostrophic (magenta) convergences of DIC and ALK. All values are averages over the North Pacific carbon sink region outlined in Figure 1. Gray shading indicates the collective uncertainty in $dpCO_2\ dt^{-1}$ due to advection.

This is consistent with the expectation that temperature effects dominate seasonal pCO_2 variability in subtropical waters [*Takahashi et al.*, 2009], as the North Pacific transition zone lies in the northern reaches of the subtropical gyre [*Ayers and Lozier*, 2010]. Though temperature effects largely determine the seasonal cycle, Figure 4 shows that taken alone they overpredict changes in pCO_2 in all seasons, indicating that other processes have meaningful roles to play in seasonal dynamics.

[54] In spring and summer, the temperature-driven increase in pCO_2 is partially offset by biological impacts, shown in green on Figure 4. In these months increased biological production and subsequent organic carbon export lowers pCO_2 in the surface mixed layer, partially offsetting the effect of warming waters. Though increased biological export of $CaCO_3$ also occurs, a process that raises pCO_2 by decreasing alkalinity, its net effect is dwarfed by that of organic carbon export.

[55] In fall and winter, temperature effects again overpredict changes in sea surface pCO_2, with cooling driving a decrease in pCO_2 larger than that which is observed. Biological impacts, though lesser in these months, nonetheless also decrease pCO_2. Physical processes are thus left to counter the temperature and biological effects, increasing pCO_2 to yield the observed. The physical processes of advection, mixing, and air-sea gas exchange all increase DIC in surface waters in these months, thus increasing sea surface pCO_2. Of these physical processes, the vertical entrainment of deep, carbon-rich waters has the greatest impact. This is evident from Table 2 and can also be seen in Figure 5, which shows changes in pCO_2 due to advection (black dashed line) broken into its Ekman, geostrophic, and vertical components. The increase in pCO_2 due to vertical convergence (yellow) is large in the fall and winter months. This is driven by the deepening of the mixed layer, entraining DIC-rich waters from depth into upper waters. As expected, in the spring and summer months, when the mixed layer shoals, this contribution approaches zero. The increase in pCO_2 due to Ekman advection (red), dominated by the horizontal transport of high-DIC subpolar waters southward into the northern subpolar gyre, contributes little to seasonal variability. Though Ekman transport is strongest in the high-wind winter months, the DIC it transports into the study region is distributed into larger mixed layer volumes in this season, thus diluting its impact on sea surface pCO_2.

[56] Though our predicted changes in pCO_2 shown in Figure 4 match the observed seasonal cycle in the North Pacific carbon sink region relatively well, they overpredict pCO_2 drawdown in the fall and into the winter. This overprediction is in part attributable to the lack of seasonal resolution in the DIC and ALK data sets, discussed in section 2.2.4 as underrepresenting fall and winter DIC values. Higher DIC values would increase pCO_2, thus acting to close the gap between our predicted changes in pCO_2 and the observed. Our overestimation of pCO_2 drawdown in fall and winter may also be due to an underestimation of vertical processes, found by *Chierici et al.* [2006] to be the primary cause for increases in mixed layer pCO_2 September through December in the western subarctic gyre. Such an underestimation could be a result of summer-biased DIC and ALK data sets. Overprediction of pCO_2 drawdown in fall and winter could also be due to overestimates of biological

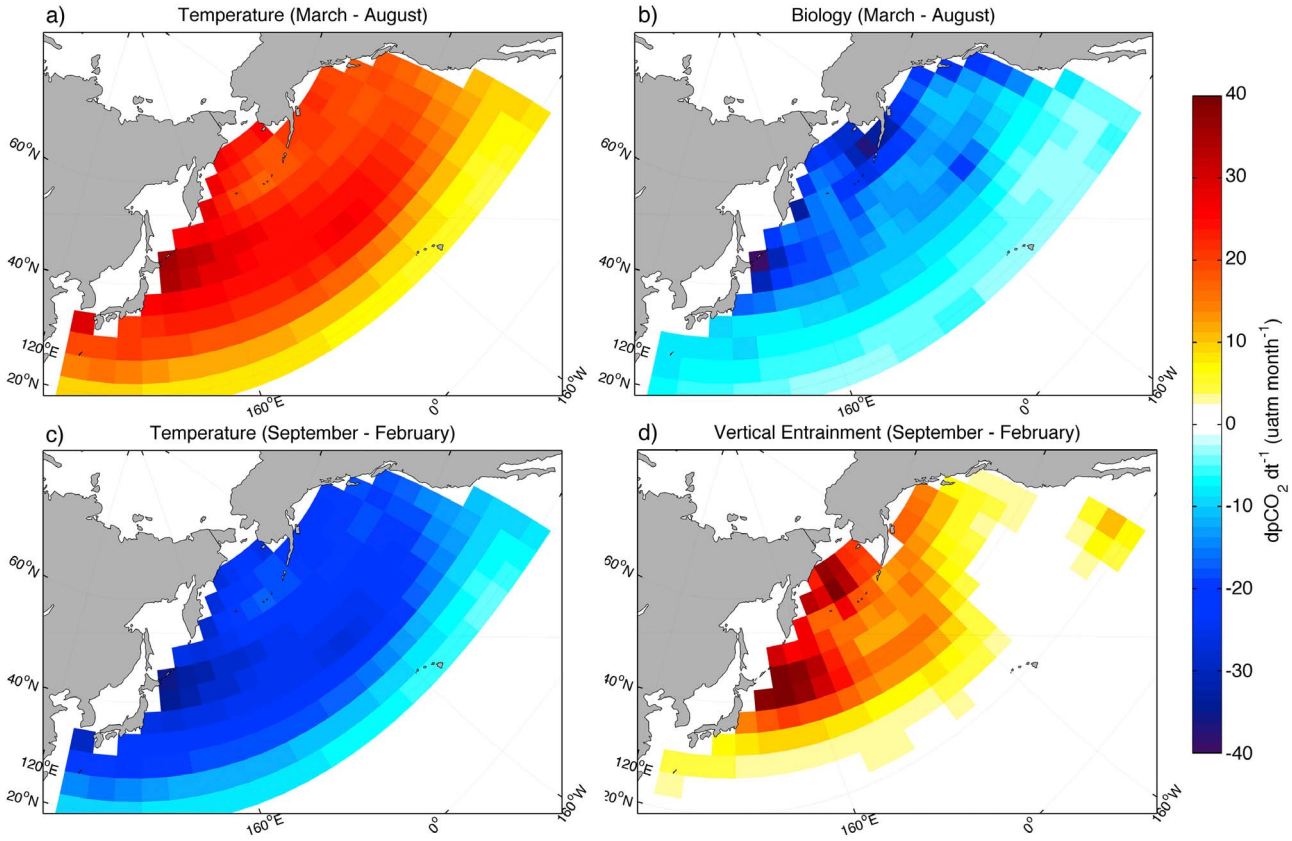

Figure 6. Dominant controls on seasonal seawater pCO_2. (a) Summer (MAMJJA) increases in pCO_2 due to warming waters are lessened by (b) high biological drawdown. (c) Winter (SONDJF) decreases in pCO_2 due to cooling waters are moderated by (d) vertical entrainment of DIC-rich waters from below.

drawdown in this season. At Ocean Station P (50°N 145°W), *Emerson and Stump* [2010] found very little net biological oxygen production in the mixed layer from September through February, indicating little organic carbon export from these waters during this time. If biological drawdown of pCO_2 in the North Pacific carbon sink region were likewise small in the fall, this might close the gap between our predicted values and the observed in this season.

[57] The dominant controls on the seasonal pCO_2 cycle in the North Pacific are summarized and shown spatially in Figure 6. Temperature effects dominate the seasonal cycle, resulting in increasing pCO_2 in the spring and summer months (March through August), and decreasing pCO_2 in the fall and winter months (September through February). In spring and summer, biological drawdown of pCO_2 partially offsets the increase due to warming. In fall and winter, the vertical entrainment of carbon-rich deep waters partially offsets the pCO_2 decrease due to cooling. Because these processes controlling pCO_2 on seasonal timescales are not necessarily those that control its annual mean state, we next consider annual controls on pCO_2.

4. Annual Controls on pCO_2

[58] To understand why this broad expanse of the North Pacific functions as a net annual carbon sink, we next consider equation (8) on a mean annual basis to reveal processes regulating sea surface pCO_2 on this time scale. Over the course of a year, seasonal increases and decreases in sea surface pCO_2 balance to yield no mean annual change in pCO_2 (equation (8), LHS). The interannual trend of increase ($\sim$1 μatm yr^{-1}) has been removed [*Takahashi et al.*, 2006, 2010]. Likewise, changes in pCO_2 due to temperature and salinity effects (RHS terms 1 and 2) are driven by seasonal cycles in these properties, and thus also balance annually, resulting in no net impact on pCO_2. Yet, the region is a sink for atmospheric CO_2 on a mean annual basis, so the positive change in pCO_2 due to air-sea flux (RHS term 6) must be balanced by a negative change in pCO_2 due to the combined effects of advection, mixing, and biology (terms 3–5).

[59] The mean annual change in sea surface pCO_2 due to each of these processes is quantified in Table 2. As expected, there is no mean annual change in observed seawater pCO_2, or in pCO_2 due to temperature effects or salinity effects. The four remaining processes, advection (composed of horizontal Ekman, geostrophic, and vertical), mixing (composed of horizontal and vertical), biology, and air-sea flux, though collectively having no net annual impact on seawater pCO_2, individually increase or decrease pCO_2 on a mean annual basis. Figures 7a–7d shows the spatial pattern of these processes: the general increase in seawater pCO_2 due to the oceanic uptake of atmospheric CO_2 (7a); the increase in pCO_2 due to mixing, driven primarily by the vertical mixing of carbon-rich waters from below (7b); the drawdown of

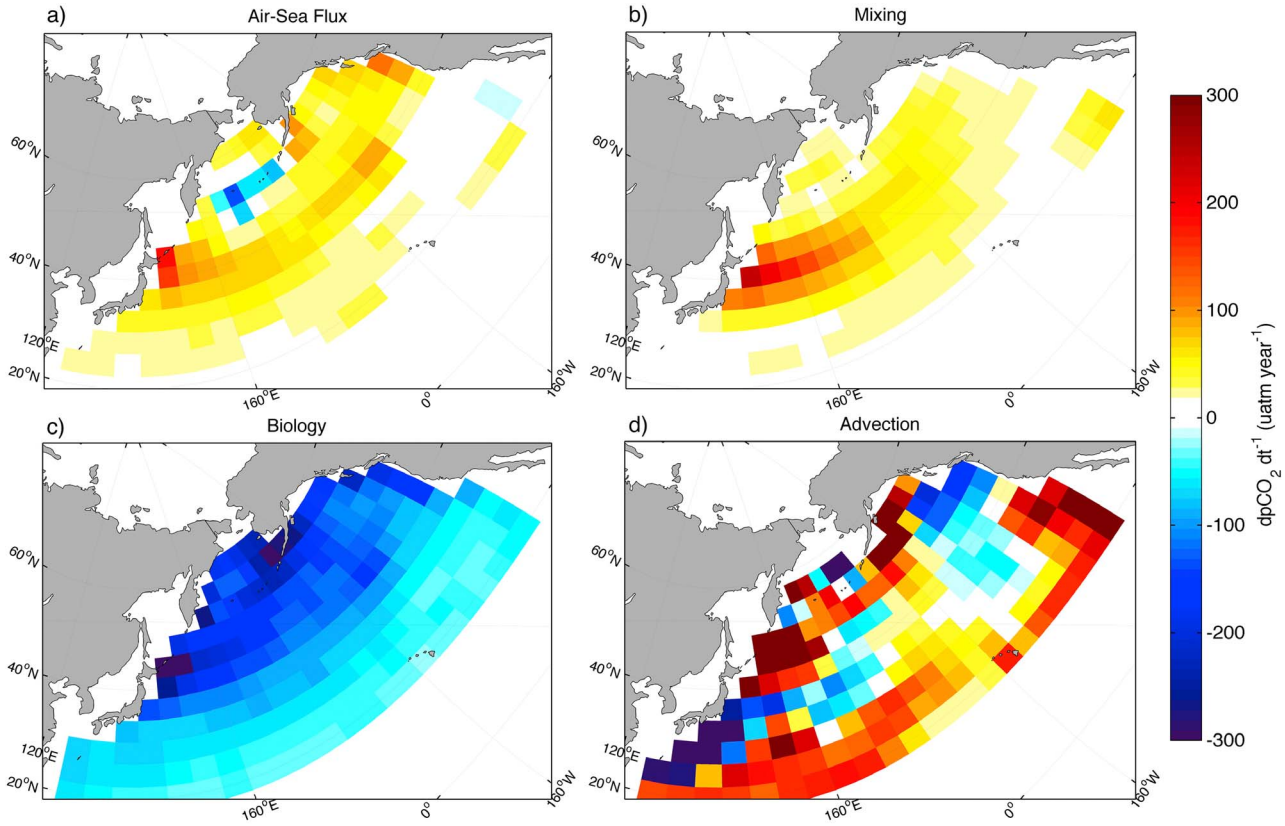

Figure 7. Processes contributing to a net annual change in sea surface pCO_2. Mean annual change in pCO_2 (μatm yr^{-1}) due to (a) air-sea CO_2 flux, (b) horizontal plus vertical mixing, (c) biological drawdown, and (d) horizontal plus vertical advection.

pCO_2 due to biological processes (7c); and the change in pCO_2 due to the combined impacts of horizontal and vertical advection, lowering pCO_2 in some regions and increasing it in others (7d).

[60] Notably absent from the annual controls on pCO_2 shown in Figure 7 is temperature, despite its dominance in driving the seasonal signal. Ostensibly, temperature has a net zero annual mean impact on pCO_2, visualized by integrating the line under the curve in Figure 4 (equation (8), RHS term 1). Though the waters warm and cool over the course of a year, their temperature always comes full circle in the mean. However, air-sea carbon flux and its effect on pCO_2 (equation (8), RHS term 6) are not independent of water temperature. Air-sea flux, given previously as $F = k\alpha\Delta pCO_2$, depends on k, the wind speed-dependent gas transfer coefficient; α, the strongly temperature-dependent solubility of CO_2 in seawater, and Δ pCO_2, the air-sea pCO_2 difference. The solubility of CO_2 is greatest in winter when the water is coldest, which is also when strong winds and a large air-sea pCO_2 difference favor oceanic uptake. Thus, via seasonal changes in solubility, temperature is expected to increase wintertime carbon uptake, and consequently the mean annual carbon sink. To what extent does this seasonal variability in solubility contribute to the carbon sink on an annual basis?

[61] To address this question, we compare (1) the observed air-sea flux, as given by *Takahashi et al.* [2009, 2010], and (2) the air-sea flux that would be expected if solubility (α) were not varying seasonally with temperature. We calculate the latter flux using the equation $F = k\alpha\Delta pCO_2$ given above, by holding solubility constant in time at its mean annual value, but allowing it to vary spatially. The observed air-sea flux which includes seasonal solubility effects (1), minus the air-sea flux calculated in the absence of seasonal solubility effects (2), yields the portion of air-sea flux resulting from just seasonal changes in solubility, shown in Figure 8a. Averaged over the study region, seasonal solubility effects account for only about 0.35 (Figure 8a) of the observed 2 mol C m^{-2} yr^{-1} (Figure 1) of atmospheric CO_2 uptake annually. Thus, in the absence of seasonal changes in solubility, the North Pacific carbon sink region would still uptake 1.65 mol C m^{-2} yr^{-1}, or 83% of the observed carbon uptake. A similar calculation, but holding the wind speed-dependent gas transfer coefficient (k) constant in time, reveals that the region would still exhibit 75% of the observed carbon uptake in the absence of seasonal wind variability.

[62] Returning to the four processes controlling sea surface pCO_2 annually (Figure 7), we can now say that a portion of those pCO_2 changes due to air-sea flux (7a) are driven by seasonal changes in the temperature-dependent solubility of CO_2 in seawater. This portion is shown in Figure 8b, which translates the air-sea flux driven by seasonal variations solubility shown in 8a into the corresponding change in sea surface pCO_2 that it drives. Note that the

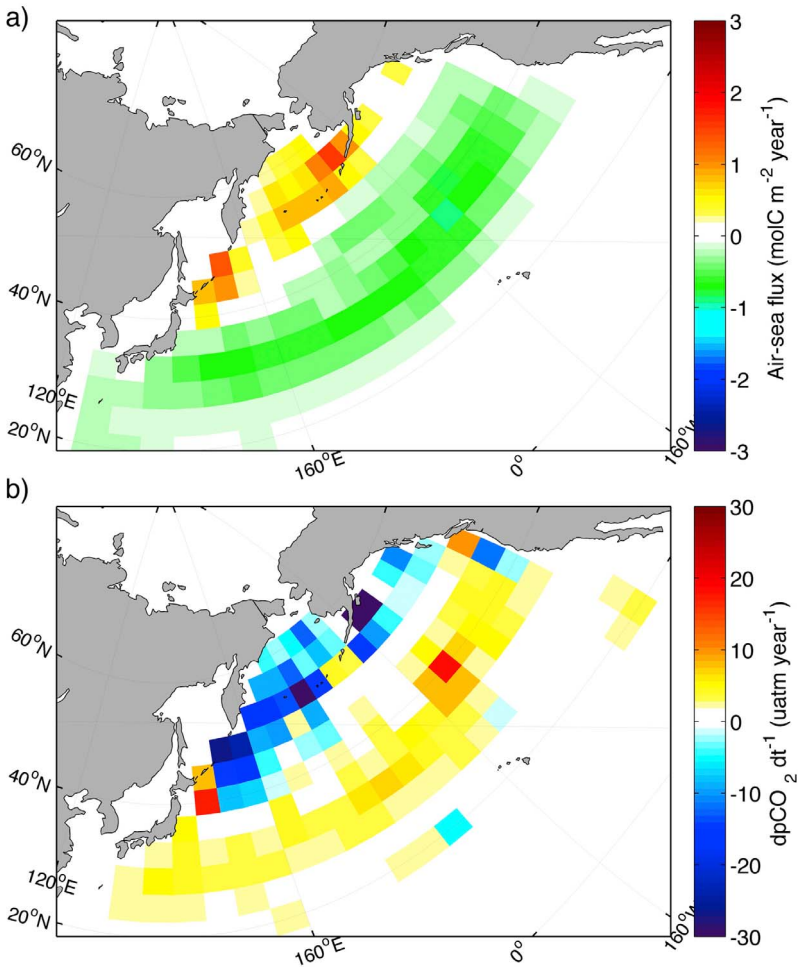

Figure 8. Contribution of seasonal solubility changes to (a) mean annual air-sea flux (mol C m^{-2} yr^{-1}), and (b) mean annual changes in sea surface pCO_2 (μatm yr^{-1}). Comparing Figure 8a with Figure 1 shows that the portion of annual air-sea flux due to seasonal solubility changes is small. Similarly, comparing Figure 8b with Figure 7a shows that the annual change in seawater pCO_2 due to seasonal solubility changes is also very small.

axis on Figure 8b is only 10% of that of Figure 7a. The influence of seasonally varying solubility on air-sea carbon flux drives a pCO_2 increase of about 2.7 μatm yr^{-1} in the study area, as compared to the total pCO_2 increase of about 61 μatm yr^{-1} that results from the air-sea flux. Thus, seasonal solubility effects account for only 4% of the mean annual increase in pCO_2 due to air-sea flux in this region. Because the oceanic carbon uptake across the air-sea boundary mixes down into the mixed layer, and solubility increases air-sea flux most in the winter when the mixed layer is deep, the seasonal solubility change has a relatively greater impact on total carbon flux than it does on resulting changes in sea surface pCO_2.

[63] Thus, though temperature dominates seasonal pCO_2 variability, it plays a minor role in determining pCO_2 on a mean annual basis: it has no direct impact annually (equation (8), RHS term 1), and only a small annual impact via the influence of seasonal solubility changes on air-sea flux (equation (8), RHS term 6). Instead, the four processes shown in Figure 7, advection, mixing, biology, and air-sea flux, regulate pCO_2 on a mean annual basis. Armed now with an understanding of seasonal and annual controls on pCO_2, we examine why the North Pacific carbon sink is where it is, and what processes maintain the region as a sink.

5. Processes Locating and Maintaining the North Pacific Carbon Sink

[64] As discussed, a wide swath across the North Pacific basin uptakes a disproportionately large amount of atmospheric carbon every year, with the region of most intense uptake located in the transitional waters in the northern reaches of the subtropical gyre, near the gyre-gyre boundary region (Figure 1). We ask two questions: (1) How does the region maintain its low sea surface pCO_2, even though it uptakes carbon year after year? and (2) What determines the location of this mean annual carbon sink?

[65] The large annual uptake of atmospheric carbon in the North Pacific is supported by those processes that remove carbon from surface waters, thus lowering sea surface pCO_2 and directing air-sea carbon flux into the ocean. As seen in Figure 7, two processes lower sea surface pCO_2 in our study region annually: biological drawdown (Figure 7c), and with some spatial heterogeneity, advection (Figure 7d). The

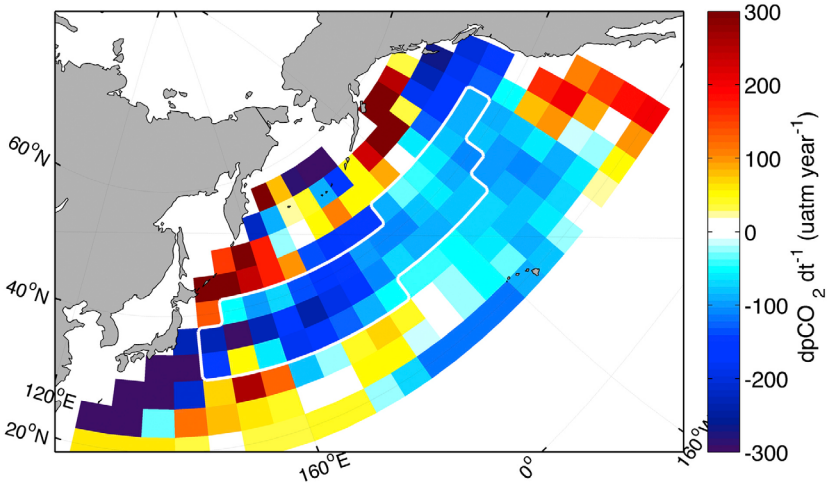

Figure 9. Mean annual change in seawater pCO_2 due to geostrophy, calculated as the change in pCO_2 due to the geostrophic divergence of DIC and ALK. Geostrophic flow lowers pCO_2 across a wide expanse of the North Pacific, and most acutely in the transition zone region. White outline indicates the study domain, as in Figure 1.

advective signal was shown broken down into its individual components previously in Figure 5. While the vertical entrainment of deep waters increases mixed layer pCO_2 in the winter, and the horizontal Ekman convergence increases pCO_2 to a lesser extent throughout the year, the geostrophic flow (magenta line) stands alone in decreasing pCO_2 in surface waters. Weak but steady, when integrated over the course of a year, the geostrophic flow lowers pCO_2 substantially (-113 ± 8 μatm yr^{-1}, Table 2). Thus, more precisely as shown by Figures 7 and 5, the two processes decreasing pCO_2 in surface waters and maintaining the carbon sink on an annual basis are biological drawdown and the geostrophic component of advection.

[66] Table 2 offers another view of the processes regulating pCO_2 on a mean annual basis, likewise showing that biology and geostrophic advection maintain the North Pacific transition zone as an annual sink. The air-sea flux of CO_2 from the atmosphere into the ocean is just one of several sources of pCO_2 to surface waters, increasing it by an estimated 61 ± 23 μatm yr^{-1} in our study region. This flux can only be maintained by processes decreasing pCO_2 on a mean annual basis. Table 2 shows only two such processes in the region: geostrophic advection, estimated to decrease pCO_2 by -113 ± 8 μatm yr^{-1}, and biological drawdown, estimated to decrease pCO_2 by approximately -111 ± 36 μatm yr^{-1}. While we acknowledge uncertainty associated with the values reported in Table 2, our conclusion is robust. Regardless of the error associated with estimates of dpCO_2 dt^{-1} due to vertical mixing, biological drawdown, air-sea flux, or any other process listed in Table 2, because the direction in which these processes impact pCO_2 is well known, biological drawdown and geostrophic advection emerge as the only processes that lower pCO_2 and thus support the oceanic uptake of CO_2 in our study region on a mean annual basis.

[67] Our finding that geostrophic advection plays a comparable role to biology in lowering pCO_2 in our study region annually is supported by the results of *Chierici et al.* [2006]. *Chierici et al.* [2006] similarly modeled CO_2 in surface waters (they use fCO_2 rather than pCO_2), but for six provinces in the subarctic North Pacific. These authors likewise accounted for changes in CO_2 due to changes in temperature, air-sea gas exchange, vertical advection and mixing, and biology. While our study additionally quantified the impacts of horizontal advection and mixing on pCO_2, Chierici et al. instead closed their mixed layer fCO_2 budget by calculating the value of a residual fCO_2 term. Their results show only two terms that lower fCO_2 across the subarctic annually: the biological impacts, and the residual term. Chierici et al. note that horizontal advection and mixing are processes likely to contribute to a carbon change, and that for their budget to be balanced, these processes must result in a net annual loss of carbon from surface waters.

[68] While the large impact of biological drawdown on sea surface pCO_2 is widely recognized, our finding that the geostrophic advection is of equal importance in lowering pCO_2 in the North Pacific carbon sink region was unexpected. Figure 9 shows the impact of geostrophic advection on pCO_2 spatially: the geostrophic flow lowers pCO_2 broadly across the basin, and most acutely west of the dateline in the Kuroshio and its extension region. This decrease in pCO_2 is driven by the geostrophic divergence of DIC. Though the geostrophic impact on pCO_2 is calculated as the change in pCO_2 resulting from the convergence or divergence of both DIC and ALK (equation (8), RHS term 3), this term is dominated by the divergence of DIC in the North Pacific carbon sink region. Figure 10 shows the mean annual geostrophic currents overlain on sea surface DIC. In the western basin, the Kuroshio carries low-DIC subtropical waters northward and eastward, creating a band of low DIC along its extension region. The North Pacific Current continues to carry these low-DIC waters across the basin, gaining atmospheric carbon along the way during most of the year. In the eastern basin, higher-DIC waters are subsequently exported laterally out of the region. This geostrophically driven, low-DIC, low-pCO_2 belt corresponds

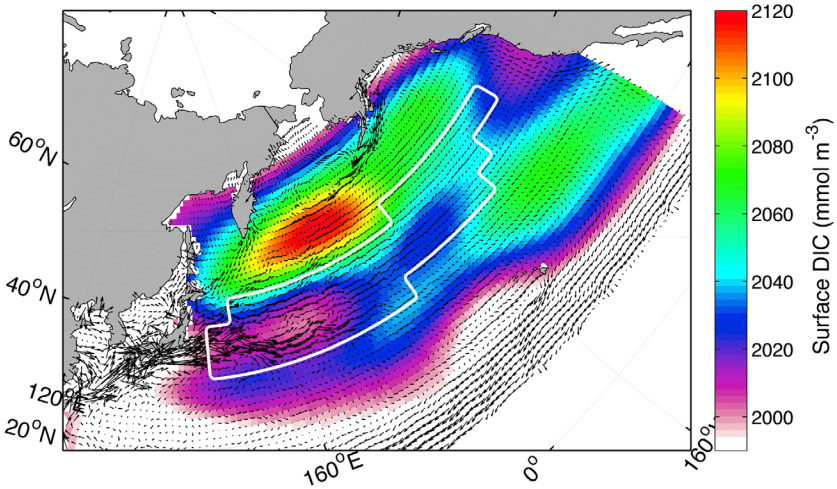

Figure 10. Mean annual geostrophic currents (black vectors) overlain on surface DIC. The Kuroshio carries large volumes of low-DIC waters eastward, creating a basin-wide band of low DIC waters in the region of the North Pacific transition zone. White outline indicates the study domain, as in Figure 1.

well to the mean annual carbon sink region, shown again outlined in white on Figure 10.

[69] The result that the geostrophic import of low-DIC and export of high-DIC waters in part maintains the North Pacific carbon sink is supported by several North Atlantic modeling studies. *Thomas et al.* [2008] found that during weak North Atlantic Oscillation (NAO) conditions, transport in the North Atlantic Current decreased, resulting in lesser transport of low-DIC waters across the basin and decreased atmospheric CO_2 uptake. Relatedly, *Ullman et al.* [2009] found that the horizontal transport of DIC drives interannual variability in air-sea flux in the transition zone waters in the North Atlantic. And finally, in an abiotic modeling study, *Follows et al.* [1996] found geostrophic flow controls CO_2 uptake in the northern part of the North Atlantic subtropical gyre by modifying the spatial pattern of pCO_2. Though processes governing carbon flux in the North Atlantic and North Pacific should not be assumed to be the same, both exhibit high uptake along the extension region of strong western boundary currents.

[70] Though the biological export of carbon vertically out of these waters, plus the lateral geostrophic removal of carbon from the region, collectively maintain the region's function as carbon sink, it is the geostrophic flow that determines its location. On a mean annual basis in the North Pacific carbon sink region, the air-sea CO_2 flux correlates strongly with the change in pCO_2 due to geostrophic flow ($r = 0.67$, $p < 0.01$) but shows no correlation with the change in pCO_2 due to biology, regardless of which of the biological parameterizations we use. Figure 11 shows this spatial relationship between air-sea CO_2 flux and the annual change in pCO_2 due to geostrophic flow. The zonal band of the largest decrease in pCO_2 (blue colormap) corresponds with the region of greatest atmospheric carbon uptake (largest black dots), occurring between ~30° and 45°N in the transition zone. Within the transition zone, geostrophy also

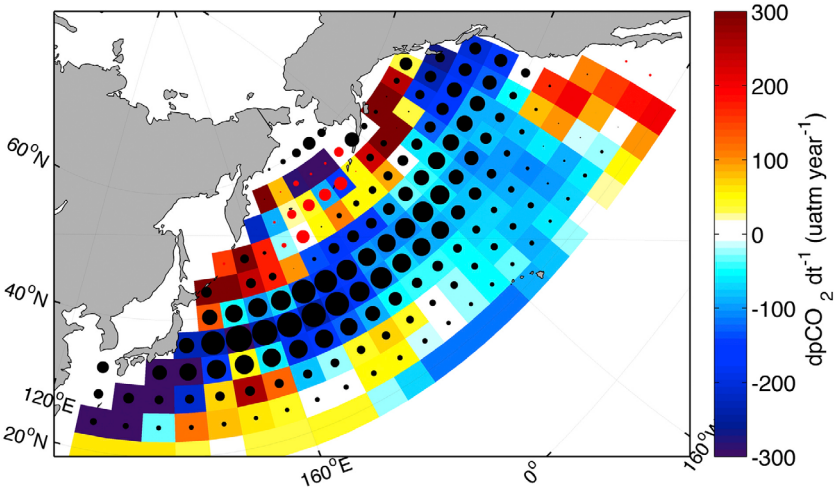

Figure 11. Mean annual change in sea surface pCO_2 due to geostrophic advection (color map), overlain by mean annual air-sea carbon flux (dots). Dot size is proportional to flux magnitude. Black stipples indicate oceanic uptake; red stipples indicate outgassing.

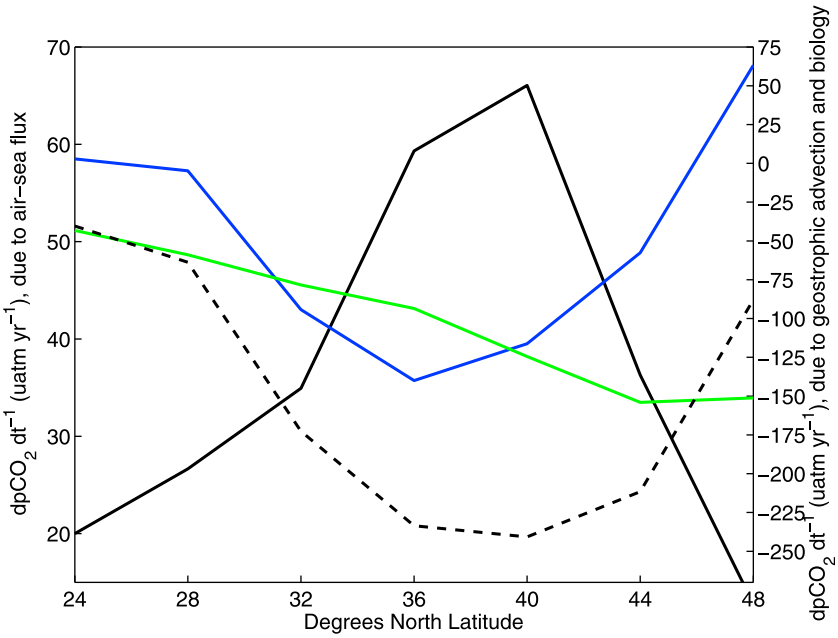

Figure 12. Mean annual change in pCO_2 by latitude, averaged from 160°E–160°W in the middle of the North Pacific carbon sink region. Left axis shows change in pCO_2 due to air-sea flux (solid black line). Right axis shows change in pCO_2 due to biology (green), geostrophic advection (blue), and biology and geostrophy combined (black dashed line). Geostrophy lowers pCO_2 disproportionately in the North Pacific transition zone (~30–45°N), driving this region to uptake large amounts of atmospheric CO_2 (shown here as its corresponding increase in pCO_2).

lowers pCO_2 to the greatest extent west of the dateline, which is also where the sink is most intense.

[71] The latitudinal control geostrophy exerts on the location of the North Pacific carbon sink is summarized graphically in Figure 12. Of the two processes lowering pCO_2 on a mean annual basis, biology (green) and geostrophic advection (blue), geostrophic advection is the only one that lowers pCO_2 disproportionately in the North Pacific transition zone, between about 30–45°N. The geostrophically lowered pCO_2 in this region supports greater air-sea carbon flux into the ocean at these latitudes, shown as the corresponding increase in pCO_2 that this flux drives (solid black). Our conclusion here, that the geostrophic advection of DIC determines the location of the North Pacific carbon sink by maintaining low pCO_2 in the region, also finds support in a North Atlantic study. Model results by *Bennington et al.* [2009] indicate that years of lower surface DIC are years of higher CO_2 influx, yet years of greater biological carbon export are not necessarily years of greater carbon uptake.

6. Summary and Conclusion

[72] This study has quantified the impact of processes regulating sea surface pCO_2, and thus atmospheric carbon dioxide uptake, in the region of the North Pacific that is a strong carbon sink on a mean annual basis. We estimated changes in pCO_2 due to temperature, salinity, advection, mixing, biology, and air-sea flux on a climatological monthly basis. From this, we determined which processes regulate the sink on seasonal and annual timescales, as well as why this particular region is a sink. Separating our work from several prior studies in the North Pacific, we quantified all processes impacting sea surface pCO_2, explicitly considering the role of large-scale ocean circulation.

[73] Processes controlling pCO_2 seasonally differ from those controlling it annually. Temperature effects dominate the seasonal pCO_2 cycle, though alone would yield greater pCO_2 extremes than observed in all seasons. In spring and summer, strong biological drawdown of pCO_2 partially offsets its increase due to warming waters. In fall and winter, the decrease in pCO_2 due to cooling is moderated primarily by the vertical entrainment of carbon-rich waters from depth.

[74] On a mean annual basis, air-sea carbon flux, biology, horizontal and vertical mixing, and horizontal and vertical advection all have a net impact on seawater pCO_2. Though temperature effects dominate seasonal variability, decreasing pCO_2 in winter and raising it proportionally in summer, this results in no net annual effect. Temperature does impact air-sea flux annually via its control on seasonal changes in the solubility of CO_2 in seawater, though this impact is modest. In the absence of seasonal solubility changes, the North Pacific carbon sink region would still exhibit 83% of the observed CO_2 uptake.

[75] The ability of the North Pacific transition zone region to uptake large amounts of atmospheric carbon year after year is maintained by both the biological export of carbon to depth and the lateral removal of carbon by geostrophic flow. Both of these processes decrease pCO_2 in surface waters on a mean annual basis, enabling the oceanic uptake of atmospheric carbon. The fate of this carbon once in the oceans remains a topic for future study; it may be temporarily sequestered in mode waters, similar to findings in the North Atlantic [*Bates et al.*, 2002], or it may be carried by the

shallow North Pacific meridional overturning circulation [*McPhaden and Zhang*, 2002, 2004] to equatorial regions where strong upwelling causes significant outgassing of CO_2 [*Takahashi et al.*, 2002, 2009].

[76] The geostrophic flow alone determines the location of the low-pCO_2 region and thus the sink, as it is the only process that lowers pCO_2 with the same latitudinal dependency as the air-sea carbon flux. Geostrophic currents bring low-DIC waters into the region and carry high-DIC waters out, driving a divergence of DIC that decreases seawater pCO_2 and supports carbon flux into the ocean at these latitudes.

[77] Though the carbon sinks located between about 20–50° latitude in the North Pacific and other basins have been attributed primarily to a combination of temperature and biological controls on seawater pCO_2 [*Takahashi et al.*, 1993, 2002, 2009], this study finds large-scale advection of DIC to also be of importance. By quantifying the impact of all processes regulating pCO_2 in the study region, we found that geostrophic circulation plays a role comparable to biological drawdown in maintaining the sink, and dominant in determining its location.

[78] Despite uncertainties associated with the time and space resolution of the data sets used, we are able to draw robust conclusions about why the North Pacific carbon sink is where it is, as well as which processes dominantly control pCO_2 in the region on what timescales. As the availability of *in situ* carbon and pCO_2 data increases, constraints on the quantitative impact of these processes will improve. Our results in the North Pacific may have a broader relevance to strong sink areas found in the same latitudinal zone in other basins, but we leave this as a topic for future investigations. It is our hope that this work can serve as a clarifying framework upon which to study other regions, as well as to improve our knowledge of this one as new data become available.

[79] **Acknowledgments.** Support for the work of J.M.A. provided by a National Defense Science and Engineering Graduate Fellowship (NDSEG), a Katherine Goodman Stern Fellowship, and a North Carolina Space Grant. Support for the work of M.S.L. provided by the National Science Foundation. The authors thank T. Westberry for generously sharing his vertically resolved productivity estimates, and Nicolas Cassar and R.T. Barber for their enthusiastic and thoughtful comments on this work.

References

Antonov, J. I., R. A. Locarnini, T. P. Boyer, A. V. Mishonov, and H. E. Garcia (2006), *World Ocean Atlas 2005*, vol. 2, *Salinity*, *NOAA Atlas NESDIS*, vol. 62, edited by S. Levitus, 182 pp., NOAA, Silver Spring, Md.

Ayers, J. M., and M. S. Lozier (2010), Physical controls on the seasonal migration of the North Pacific transition zone chlorophyll front, *J. Geophys. Res.*, *115*, C05001, doi:10.1029/2009JC005596.

Bates, N., A. C. Pequignet, R. J. Johnson, and N. Gruber (2002), A short-term sink for atmospheric CO_2 in subtropical mode water in the North Atlantic Ocean, *Nature*, *420*, 489–493, doi:10.1038/nature01253.

Behrenfeld, M. J., and P. G. Falkowski (1997), Photosynthetic rates derived from satellite-based chlorophyll concentration, *Limnol. Oceanogr.*, *42*, 1–20, doi:10.4319/lo.1997.42.1.0001.

Bennington, V., G. A. McKinley, S. Dutkiewicz, and D. Ullman (2009), What does chlorophyll variability tell us about export and air-sea CO_2 flux variability in the North Atlantic?, *Global Biogeochem. Cycles*, *23*, GB3002, doi:10.1029/2008GB003241.

Brewer, P. G., and J. C. Goldman (1976), Alkalinity changes generated by phytoplankton growth, *Limnol. Oceanogr.*, *21*(1), 108–117, doi:10.4319/lo.1976.21.1.0108.

Brewer, P. G., G. T. F. Wong, M. P. Bacon, and D. W. Spencer (1975), An oceanic calcium problem?, *Earth Planet. Sci. Lett.*, *26*, 81–87, doi:10.1016/0012-821X(75)90179-X.

Brohan, P., J. J. Kennedy, I. Harris, S. F. B. Tett, and P. D. Jones (2006), Uncertainty estimates in regional and global observed temperature changes: A new data set from 1950, *J. Geophys. Res.*, *111*, D12106, doi:10.1029/2005JD006548.

Byrne, R. H., S. Mecking, R. A. Feely, and X. Liu (2010), Direct observations of basin-wide acidification of the North Pacific Ocean, *Geophys. Res. Lett.*, *37*, L02601, doi:10.1029/2009GL040999.

Carlson, C. A., H. W. Ducklow, and A. F. Michaels (1994), Annual flux of dissolved organic carbon from the euphotic zone in the Northwestern Sargasso Sea, *Nature*, *371*, 405–408, doi:10.1038/371405a0.

Chierici, M., A. Fransson, and Y. Nojiri (2006), Biogeochemical processes as drivers of surface fCO_2 in contrasting provinces in the subarctic North Pacific Ocean, *Global Biogeochem. Cycles*, *20*, GB1009, doi:10.1029/2004GB002356.

Dickson, A. G., and F. J. Millero (1987), A comparison of the equilibrium constants for the dissociation of carbonic acid in seawater media, *Deep Sea Res., Part A*, *34*, 1733–1743, doi:10.1016/0198-0149(87)90021-5.

Dore, J. E., R. Lukas, D. W. Sadler, and D. M. Karl (2003), Climate-driven changes to the atmospheric CO_2 sink in the subtropical North Pacific Ocean, *Nature*, *424*, 754–757, doi:10.1038/nature01885.

Dunne, J. P., R. A. Armstrong, A. Gnanadesikan, and J. L. Sarmiento (2005), Empirical and mechanistic models for the particle export ratio, *Global Biogeochem. Cycles*, *19*, GB4026, doi:10.1029/2004GB002390.

Emerson, S., and C. Stump (2010), Net biological oxygen production in the ocean–II: Remote in situ measurements of O_2 and N_2 in subarctic Pacific surface waters, *Deep Sea Res., Part II*, *57*, 1255–1265, doi:10.1016/j.dsr.2010.06.001.

Emerson, S., P. Quay, D. Karl, C. Winn, L. Tupas, and M. Landry (1997), Experimental determination of the organic carbon flux from open-ocean surface waters, *Nature*, *389*, 951–954, doi:10.1038/40111.

Emerson, S., C. Sabine, M. F. Cronin, R. A. Feely, S. E. Cullison Gray, and M. DeGrandpre (2011), Quantifying the flux of $CaCO_3$ and organic carbon from the surface ocean using in situ measurements of O_2, N_2, pCO_2, and pH, *Global Biogeochem. Cycles*, *25*, GB3008, doi:10.1029/2010GB003924.

Follows, M. J., R. G. Williams, and J. C. Marshall (1996), The solubility pump of carbon in the subtropical gyre of the North Atlantic, *J. Mar. Res.*, *54*, 605–630, doi:10.1357/0022240963213682.

Goldman, J. C., and P. G. Brewer (1980), Effect of nitrogen source and growth rate on phytoplankton-mediated changes in alkalinity, *Limnol. Oceanogr.*, *25*(2), 352–357, doi:10.4319/lo.1980.25.2.0352.

Goyet, C., R. J. Healy, and J. P. Ryan (2000), Global distribution of total inorganic carbon and total alkalinity velow the deepest winter mixed layer depths, 40 pp., U.S. Dep. of Energy, Oak Ridge, Tenn.

Hopkinson, C. S., and J. Vallino (2005), Efficient export of carbon to the deep ocean through dissolved organic matter, *Nature*, *433*, 142–145, doi:10.1038/nature03191.

Howard, E., S. Emerson, S. Bushinsky, and C. Stump (2010), The role of net community production in the air-sea carbon fluxes at the North Pacific subarctic-subtropical boundary region, *Limnol. Oceanogr.*, *55*, 2585–2596, doi:10.4319/lo.2010.55.6.2585.

Juranek, L. W. (2007), Assessment of Pacific Ocean organic carbon production and export using measurements of dissolved oxygen isotopes and oxygen/argon gas ratios, PhD dissertation, 154 pp., Univ. of Wash., Seattle.

Kakinoki, K., S. Imawaki, H. Uchida, H. Nakamura, K. Ichikawa, S. Umatani, A. Nishina, H. Ichikawa, and M. Wimbush (2008), Variations of Kuroshio geostrophic transport south of Japan estimated from long-term IES observations, *J. Oceanogr.*, *64*, 373–384, doi:10.1007/s10872-008-0030-4.

Karl, D., R. Letelier, J. Dore, J. Christian, and D. Hebel (1997), The role of nitrogen fixation in the biogeochemical cycling in the subtropical North Pacific Ocean, *Nature*, *388*, 533–538, doi:10.1038/41474.

Keeling, C. D., S. C. Piper, R. B. Bacastow, M. Wahlen, T. P. Whorf, M. Heimann, and H. A. Meijer (2001), *Exchanges of Atmospheric CO_2 and $^{13}CO_2$ With the Terrestrial Biosphere and Oceans From 1978 to 2000, I. Global aspects, SIO Ref. Ser., No. 01-06*, 88 pp., Scripps Inst. of Oceanogr., San Diego, Calif. [Available at http://scrippsco2.ucsd.edu/data/atmospheric_co2.html.]

Key, R. M., A. Kozyr, C. L. Sabine, K. Lee, R. Wanninkhof, J. L. Bullister, R. A. Feely, F. J. Millero, C. Mordy, and T.-H. Peng (2004), A global ocean carbon climatology: Results from Global Data Analysis Project (GLODAP), *Global Biogeochem. Cycles*, *18*, GB4031, doi:10.1029/2004GB002247.

Kimura, S., A. Kasai, H. Nakata, T. Sugimoto, J. H. Simpson, and J. V. S. Choek (1997), Biological productivity of meso-scale eddies caused by frontal disturbances in the Kuroshio, *ICES J. Mar. Sci.*, *54*, 179–192.

Kimura, S., H. Nakata, and Y. Okazaki (2000), Biological production in meso-scale eddies caused by frontal disturbances of the Kuroshio Extension, *ICES J. Mar. Sci.*, *57*, 133–142, doi:10.1006/jmsc.1999.0564.

Laws, E. A., P. G. Falkowski, W. O. J. Smith, H. Ducklow, and J. J. McCarthy (2000), Temperature effects on export production in the open ocean, *Global Biogeochem. Cycles*, *14*, 1231–1246, doi:10.1029/1999GB001229.

Lee, K. (2001), Global net community production estimated from the annual cycle of surface water total dissolved inorganic carbon, *Limnol. Oceanogr.*, *46*, 1287–1297, doi:10.4319/lo.2001.46.6.1287.

Locarnini, R. A., A. V. Mishonov, J. I. Antonov, T. P. Boyer, and H. E. Garcia (2006), *World Ocean Atlas 2005, Temperature, NOAA Atlas NESDIS*, vol. 1, edited by S. Levitus, 182 pp., NOAA, Silver Spring, Md.

McKinley, G. A., et al. (2006), North Pacific carbon cycle response to climate variability on seasonal to decadal timescales, *J. Geophys. Res.*, *111*, C07S06, doi:10.1029/2005JC003173.

McPhaden, M. J., and D. Zhang (2002), Slowdown of the meridional overturning circulation in the upper Pacific Ocean, *Nature*, *415*, 603–608, doi:10.1038/415603a.

McPhaden, M. J., and D. Zhang (2004), Pacific Ocean circulation rebounds, *Geophys. Res. Lett.*, *31*, L18301, doi:10.1029/2004GL020727.

Milliman, J. D., and P. J. Troy (1999), Biologically mediated dissolution of calcium carbonate above the chemical lysocline?, *Deep Sea Res., Part I*, *46*, 1653–1669, doi:10.1016/S0967-0637(99)00034-5.

Noriki, S., S. Otosaka, and S. Tsunogai (1999), Particulate fluxes at station KNOT in the western North Pacific during 1988–1991, in *Proceedings in the Second International Symposium on CO_2* in the Oceans, edited by Y. Nojiri, pp. 331–337, Terra Sci., Tsukuba, Japan.

Ogawa, H., and E. Tanoue (2003), Dissolved organic matter in oceanic waters, *J. Oceanogr.*, *59*, 129–147, doi:10.1023/A:1025528919771.

Ogawa, K., T. Usui, S. Takatani, T. Kitao, T. Harimoto, S. Katoh, S. Dobashi, T. Midorikawa, H. Y. Inoue, and Y. Dokiya (2006), Shipboard measurements of atmospheric and surface seawater pCO_2 in the North Pacific carried out from January 1999 to October 2000 on the voluntary observation ship MS Alligator Liberty, *Pap. Meteorol. Geophys*, *57*, 37–46, doi:10.2467/mripapers.57.37.

Roden, G. I. (1991), Subarctic-subtropical transition zone of the North Pacific: Large-scale aspects and mesoscale structure, in *Biology, Oceanography, and Fisheries of the North Pacific Transition Zone and Subartic Frontal Zone*, *Tech. Rep. NMFS 105*, 38 pp., NOAA, Silver Spring, Md.

Rodgers, K. B., J. L. Sarmiento, O. Aumont, C. Crevoisier, C. de Boyer Montegut, and N. Metzl (2008), A wintertime uptake window for anthropogenic CO_2 in the North Pacific, *Global Biogeochem. Cycles*, *22*, GB2020, doi:10.1029/2006GB002920.

Sabine, C. L., et al. (2004), The oceanic sink for anthropogenic CO_2, *Science*, *305*, 367–371, doi:10.1126/science.1097403.

Sabine, C. L., R. M. Key, A. Kozyr, R. A. Feely, R. Wanninkhof, F. J. Millero, T.-H. Peng, J. L. Bullister, and K. Lee (2005), Global Ocean Data Analysis Project: Results and data, *Tech. Rep. ORNL/CDIAC-145/NDP-083*, 110 pp., Carbon Dioxide Inf. Anal. Cent., Oak Ridge Natl. Lab., Oak Ridge, Tenn.

Sarmiento, J. L., and N. Gruber (2006), *Ocean Biogeochemical Dynamics*, 526 pp., Princeton Univ. Press, Princeton, N. J.

Sarmiento, J. L., J. Dunne, A. Gnanadesikan, R. M. Key, K. Matsumoto, and R. Slater (2002), A new estimate of the $CaCO_3$ to organic carbon export ratio, *Global Biogeochem. Cycles*, *16*(4), 1107, doi:10.1029/2002GB001919.

Stevenson, J. W., and P. P. Niiler (1983), Upper ocean heat budget during the Hawaii-to-Tahiti shuttle experiment, *J. Phys. Oceanogr.*, *13*, 1894–1907, doi:10.1175/1520-0485(1983)013<1894:UOHBDT>2.0.CO;2.

Stoll, M. H. C., H. M. van Aken, H. J. W. de Baar, and C. J. de Boer (1996), Meridional carbon dioxide transport in the northern North Atlantic, *Mar. Chem.*, *55*, 205–216, doi:10.1016/S0304-4203(96)00057-6.

Swenson, M. S., and D. V. Hansen (1999), Tropical Pacific Ocean mixed layer heat budget: The Pacific cold tongue, *J. Phys. Oceanogr.*, *29*, 69–81, doi:10.1175/1520-0485(1999)029<0069:TPOMLH>2.0.CO;2.

Takahashi, T., J. Olafsson, J. G. Goddard, D. W. Chipman, and S. C. Sutherland (1993), Seasonal variation of CO_2 and nutrients in the high-latitude surface oceans: A comparative study, *Global Biogeochem. Cycles*, *7*, 843–878, doi:10.1029/93GB02263.

Takahashi, T., et al. (2002), Global sea-air CO_2 flux based on climatological surface ocean pCO_2, and seasonal biological and temperature effects, *Deep Sea Res., Part II*, *49*, 1601–1622, doi:10.1016/S0967-0645(02)00003-6.

Takahashi, T., S. C. Sutherland, R. A. Feely, and R. Wanninkhof (2006), Decadal change of the surface water pCO_2 in the North Pacific: A synthesis of 35 years of observations, *J. Geophys. Res.*, *111*, C07S05, doi:10.1029/2005JC003074.

Takahashi, T. S., et al. (2009), Climatological mean and decadal change in surface ocean pCO_2, and net sea-air CO_2 flux over the global oceans, *Deep Sea Res. II*, *56*, 544–577, doi:10.1016/j.dsr2.2008.12.009.

Takahashi, T., S. C. Sutherland, and A. Kozyr (2010), Global ocean surface water partial pressure of CO_2 database: Measurements performed during 1957–2009 (version 2009), *Tech. Rep. ORNL/CDIAC-152, NDP-088 (V2009)*, Carbon Dioxide Inf. Anal. Cent., Oak Ridge Natl. Lab., U.S. Dep. of Energy, Oak Ridge, Tenn.

Thomas, H., A. E. Friederike Prowe, I. D. Lima, S. C. Doney, R. Wanninkhof, R. J. Greatbatch, U. Schuster, and A. Corbière (2008), Changes in the North Atlantic Oscillation influence CO_2 uptake in the North Atlantic over the past 2 decades, *Global Biogeochem. Cycles*, *22*, GB4027, doi:10.1029/2007GB003167.

Tsurushima, N., Y. Nojiri, K. Imai, and S. Watanabe (2002), Seasonal variations of carbon dioxide system and nutrients in the surface mixed layer at station KNOT (44°N, 155°E) in the subarctic western North Pacific, *Deep Sea Res., Part II*, *49*, 5377–5394, doi:10.1016/S0967-0645(02)00197-2.

Ullman, D. J., G. A. McKinley, V. Bennington, and S. Dutkiewicz (2009), Trends in the North Atlantic carbon sink: 1992–2006, *Global Biogeochem. Cycles*, *23*, GB4011, doi:10.1029/2008GB003383.

van Heuven, S., D. Pierrot, E. Lewis, and D. W. R. Wallace (2009), MATLAB program developed for CO_2 system calculations, *Tech. Rep. ORNL/CDIAC-105b*, Carbon Dioxide Inf. Anal. Cent., Oak Ridge Natl. Lab., U.S. Dep. of Energy, Oak Ridge, Tenn.

Visbeck, M., J. Marshall, T. Haine, and M. Spall (1997), Specification of eddy transfer coefficients in coarse-resolution ocean circulation models, *J. Phys. Oceanogr.*, *27*, 381–402, doi:10.1175/1520-0485(1997)027<0381:SOETCI>2.0.CO;2.

Webb, D. J., and N. Suginohara (2001), Vertical mixing in the ocean, *Nature*, *409*, 37, doi:10.1038/35051171.

Westberry, T., M. J. Behrenfeld, D. A. Siegel, and E. Boss (2008), Carbon-based primary productivity modeling with vertically resolved photoacclimation, *Global Biogeochem. Cycles*, *22*, GB2024, doi:10.1029/2007GB003078.

Wong, C. S., N. A. D. Waser, Y. Nojiri, W. K. Johnson, F. A. Whitney, J. S. C. Page, and J. Zeng (2002a), Seasonal and interannual variability in the distribution of surface nutrients and dissolved inorganic carbon in the northern North Pacific: Influence of El Nino, *J. Oceanogr.*, *58*, 227–243, doi:10.1023/A:1015897323653.

Wong, C. S., N. A. D. Waser, Y. Nojiri, F. A. Whitney, J. S. Page, and J. Zeng (2002b), Seasonal cycles of nutrients and dissolved inorganic carbon at high and mid latitudes in the North Pacific Ocean during the *Skaugran* cruises: Determination of new production and nutrient uptake ratios, *Deep Sea Res., Part II*, *49*, 5317–5338, doi:10.1016/S0967-0645(02)00193-5.

Wong, C. S., N. A. D. Waser, F. A. Whitney, W. K. Johnson, and J. S. Page (2002c), Time-series study of the biogeochemistry of the North East subarctic Pacific: Reconciliation of the C_{org}/N remineralization and uptake ratios with the Redfield ratios, *Deep Sea Res., Part II*, *49*, 5717–5738, doi:10.1016/S0967-0645(02)00211-4.

Yamanaka, Y., and E. Tajika (1996), The role of the vertical fluxes of particulate organic matter and calcite in the ocean carbon cycle: Studies using an ocean biogeochemical general circulation model, *Global Biogeochem. Cycles*, *10*, 361–382, doi:10.1029/96GB00634.

Zeebe, R. E., and D. A. Wolf-Gladrow (2001), *CO_2 in Seawater: Equilibrium, Kinetics, Isotopes*, *Elsevier Oceanogr. Ser.*, vol. 65, 360 pp., Elsevier, Amsterdam.

J. M. Ayers, Institute for Marine and Antarctic Studies, University of Tasmania, Private Bag 129, Hobart, Tas 7001, Australia. (jennifer.ayers@utas.edu.au)

M. S. Lozier, Department of Earth and Ocean Sciences, Nicholas School of the Environment, Duke University, Durham, NC 27708, USA.